Chapter 1

Imaging in Ophthalmology

Umit Yolcu, Omer Faruk Sahin and
Fatih C. Gundogan

Additional information is available at the end of the chapter

http://dx.doi.org/10.5772/58314

1. Introduction

The imaging systems have a unique role in the ophthalmologic routine practice. While imaging has an auxiliary role in other branches of medicine, it is the most essential part of the ophthalmic examination. In other words, it can be said that ophthalmic examination is almost impossible without imaging. In this chapter, a basic review of the essentials of imaging techniques in ophthalmology will be presented.

2. Anterior segment imaging systems

2.1. Slit-lamp biomicroscopy

The slit lamp biomicroscopy is an important tool in ophthalmic practice. It is basically designed for examination of anterior segment but with the appropriate attachments, all ocular structures can be viewed. Most important advantage of biomicroscopy in examining the eye structures is stereopsis, in other words ophthalmologist can examine eye structures in three dimensions. It is a routine examination tool of most practitioners. In order to use all benefits of this tool, clinician should understand the basic imaging principle of the instrument.

Modern slit-lamp biomicroscopes have two major parts; observation and illumination systems. The illumination system of slit lamp projects bright slit light onto the focus plane. Illumination part delivers very sharp, thin and undistorted slit light in order to view true representation of the ocular structures. Blue and green filters are available in most slit-lamps to visualize fluorescein stain, micro-aneurysms and nerve fiber layer. In recent years LED illuminated slit lamps are also available. LED illuminated systems provides sharpest, brightest and most

homogeneous slit beam. The other advantages LED systems on halogen lamps are last 100 times longer, have special light spectrum and they consume less energy.

Observation part comprises many optical lenses in order to deliver magnified view of ocular structures. Its magnification range differs between 5x to 40x depending on the manufacturer (Figure 1 A-F). It can enable magnification by flip-type, Galilean rotating barrel and continuous zoom methods [1]. High magnified view may be desirable for many clinicians however image quality compromises with high magnification. Therefore least required magnification should be used for the examination to achieve the best possible resolution. Resolution of a slit-lamp is depends on the wavelength of light used, the refractive index between the eye and objective, the working distance, and the diameter of the objective lens. Most biomicroscope oculars have 10 to 15 degree convergence angle to minimize convergence need of the examiner during the examination.

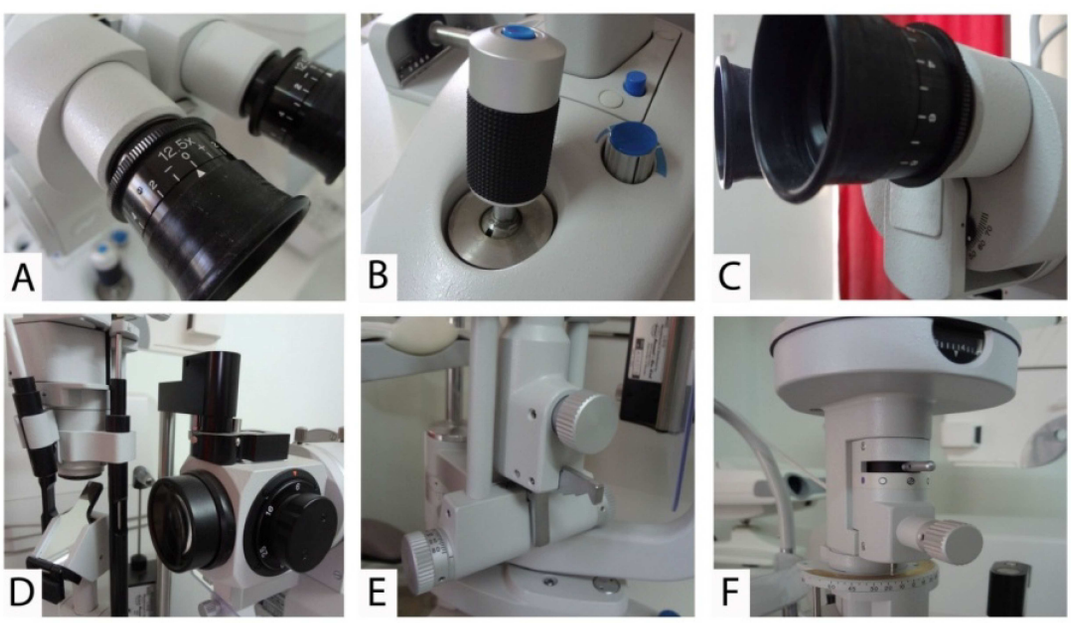

Figure 1. A. Binocular eyepieces provide stereoscopic vision and can be adjusted for examiners refraction. B. Joystick allows focusing with movement to forward, backward, laterally and diagonally. It can be rotated to lower or elevate the light beam. C. Eyepieces can be adjusted for Interpupillar distance of examiner D. Magnification can be changed with between 6x to 40 x. E. Releasing the knob allows separation of illumination and observation point. F. Slit height, color and angle can be adjusted with knurled knob.

In normal usage illumination system and observation system are coupled on a common focal plane and point. Both moves around a common focus point. It can horizontally uncoupled by releasing a knob. It is recommended that before using the slit lamp, distance between eyepieces should be adjusted for inter pupillary distance of the practitioner and focused by the help of a rod for his or her refraction. This procedure helps comfortable binocular viewing. Examination also should be conducted in semi-dark light conditions.

http://dx.doi.org/10.5772/58314

2.1.1. Examination techniques

2.1.1.1. Diffuse illumination

Diffuse illumination is a simple illumination method for examining the eye and surrounding structures. Slit width should be set to maximum, magnification to low and light at approximately 45-degree (Figure 2). Details cannot be viewed by this method; it just gives overview of eye and adnexia. High magnification should not be used with this method. Corneal scars, foreign bodies, pigmentary changes should be noted by this gross inspection method [2]. Findings obtained by the diffuse illumination should be investigated by other illumination techniques.

Cobalt blue filter and red free (green) filter can be used with this method. After instillation of fluorescein stain corneal epithelial defects, tear break up time and contact lens positioning can be viewed under cobalt blue light. With the green filter, bulbar conjunctival vessels and small hemorrhages and aneurysms can be viewed.

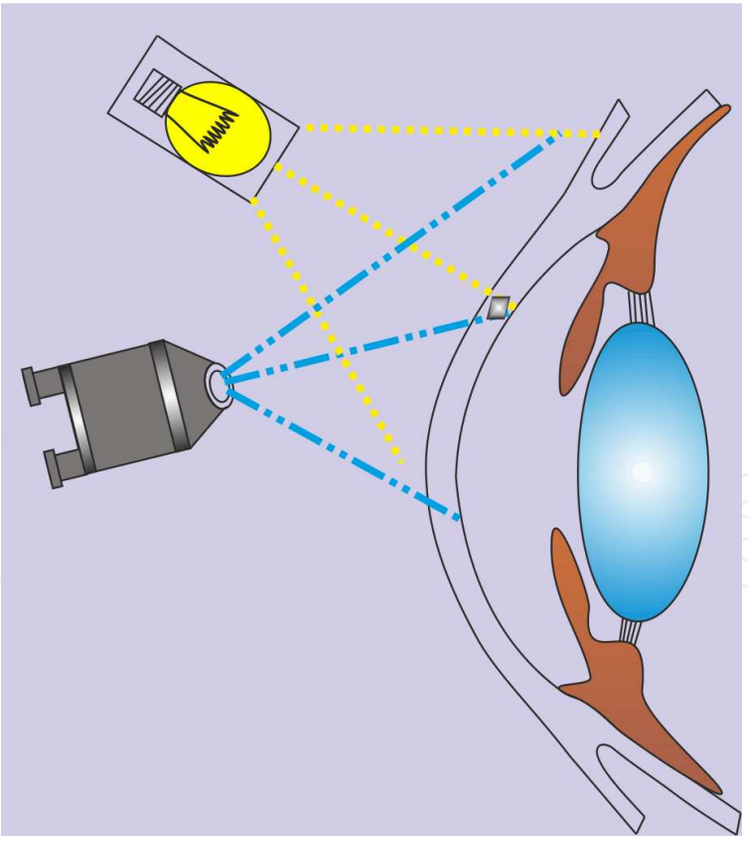

Figure 2. Diffuse illumination

a. Direct Illumination

Direct focal illumination is the most commonly used method. Observer focuses on the area directly illuminated by the slit light. Magnification can be increased to maximum if needed. Direct illumination can be used with different type of light beams.

Optic section of the cornea, anterior chamber and lens can be examined with optic section technique. Depth of any foreign body, stromal thinning, epithelial edema, layers of cornea, anterior chamber depth and different layers of lens can be determined. In this technique, illumination system is placed on the side of cornea or lens (i.e. temporal) and is set at angle between 30-60 degrees. Light beam is narrowed to minimum, light intensity is adjusted to maximum. Then examiner should focus on the middle point of horizontal corneal or lens section. Middle or maximum magnification can be used (Figure 3) [2].

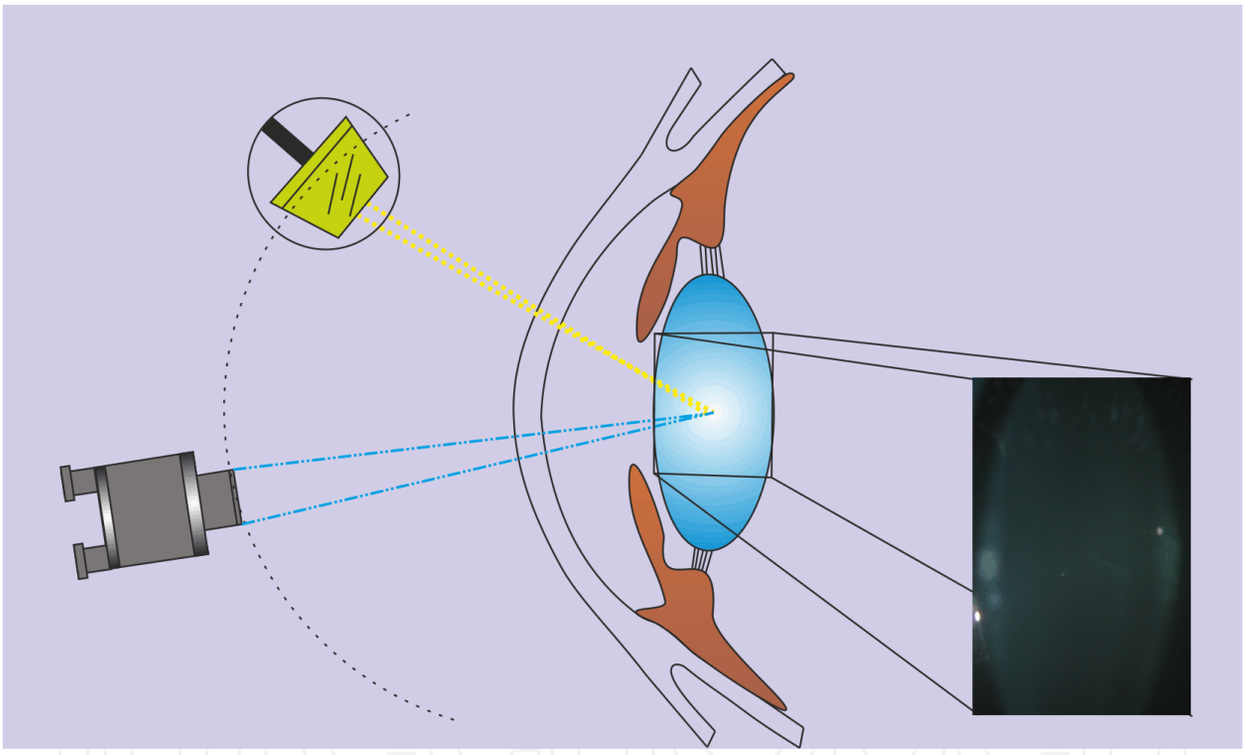

Figure 3. Direct illumination, optic section technique.

Parallelepiped technique provides detection of any condition which obscures corneal transparency or crystalline lens. In this technique illumination system is placed on the side of cornea or lens (i.e. temporal) and light beam is widened to corneal depth (3-4 mm). By this way a parallelepiped illuminated area is created. Angle can be changed between 30-60 degrees. Magnification may vary between 10x-40x (Figure 4). By focusing on the anterior side of the parallelepiped light, corneal epithelial alterations and protein deposits and debris in a contact lens wearer can be viewed. Endetolial pigment changes, keratic precipitates, other deposits and striations on the endotelium can be viewed by using parallelepiped technique [2].

http://dx.doi.org/10.5772/58314

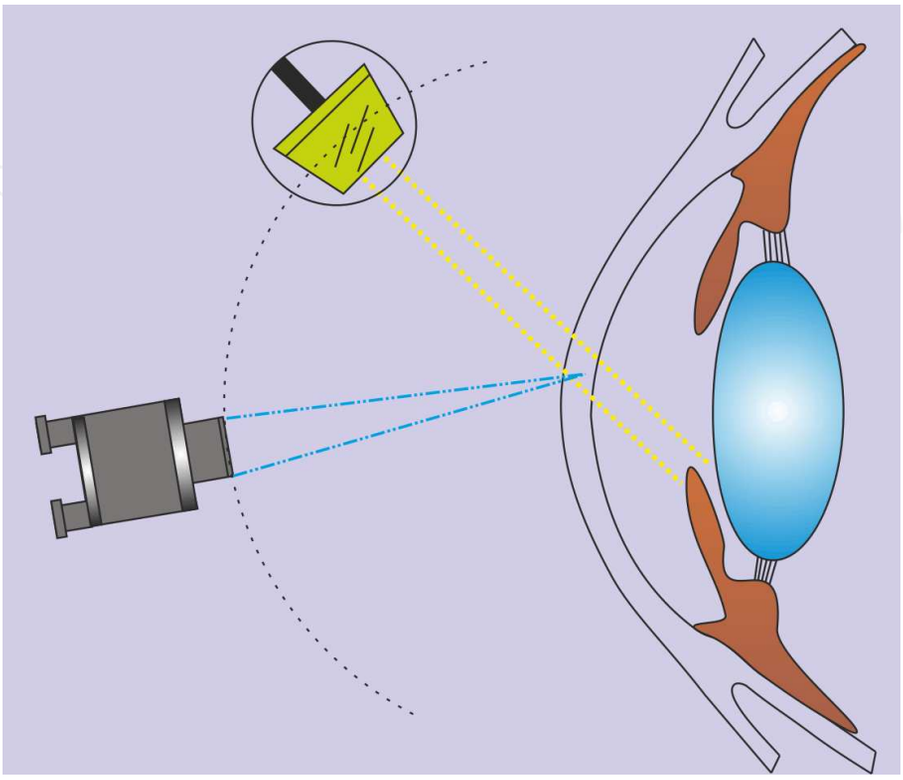

Figure 4. Direct illumination, parallelepiped technique

Crystalline lens transparency and opacities can be evaluated by using with a 0.5 to 2 mm wide beam. Different from the corneal examination illumination, system should be set to a smaller angle, 10 to 45 degree. Detailed examination can be performed by directing the light towards the pupil area and focusing different layers of the lens [2].

Wide beam illumination is useful for the inspection of contact lens surface. By this method, protein deposits, mucus secretion, corneal nerve fibers, infiltrative keratitis, corneal opacities, iris and lens surface can be viewed. Setup of the method is similar to parallelepiped method except slit width is wider then corneal depth. Light intensity should get reduced and angle of the illumination adjusted depending on the surface of under inspection, generally more than 45 degrees [2].

Conical beam illumination is useful in viewing the inflammatory cells and proteins in the anterior chamber. In this method width and height of the slit light beam is reduced until obtaining a point light. Height is reduced to 1-2 mm. Light intensity is set to maximum. Examination should be done in dark conditions (Figure 5) [2]. The number of cells in the anterior chamber is assessed from side to side of the anterior chamber in medium magnification and high-angle illumination.

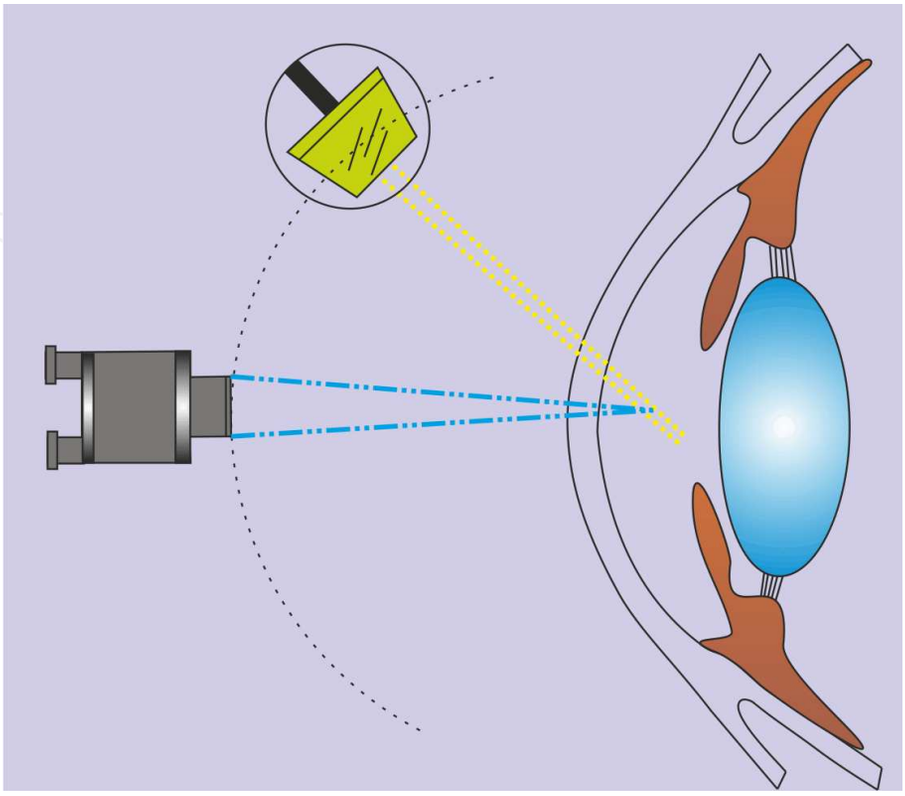

Figure 5. Conical beam illumination

b. Indirect illumination

In this technique light beam is projected to a different area other than the focal point of the observation system. Illumination system is get moved off from its click position by releasing a knob (Figure 6). Therefore two systems do not coincide at same point. Procedure is similar to parallelepiped illumination technique exceptionally, in this method, observed area is not directly the illuminated area but just beside the anterior border of parallelepiped area. With this method, transparency loss or loose contrast differences in transparent structures can be viewed such as subtle corneal opacities, bulbar conjunctival vessels and lens opacities [2].

Scleral scatter is used for especially small changes in large transparent areas. Central corneal clouding, bullous keratopathy, corneal scars, contact lens edges can be examined with this method. In this method, parallelepiped beam focused on central cornea then after releasing the knob illumination system moved out its click position and beam can be projected to nasal or temporal limbus (Figure 7). With correct positioning of the illumination system, a halo of scatter light around the cornea can be viewed [2]. Any condition which alters corneal transparency obstructs the internal reflecting light and becomes visible as a whitish color over pupil background.

http://dx.doi.org/10.5772/58314

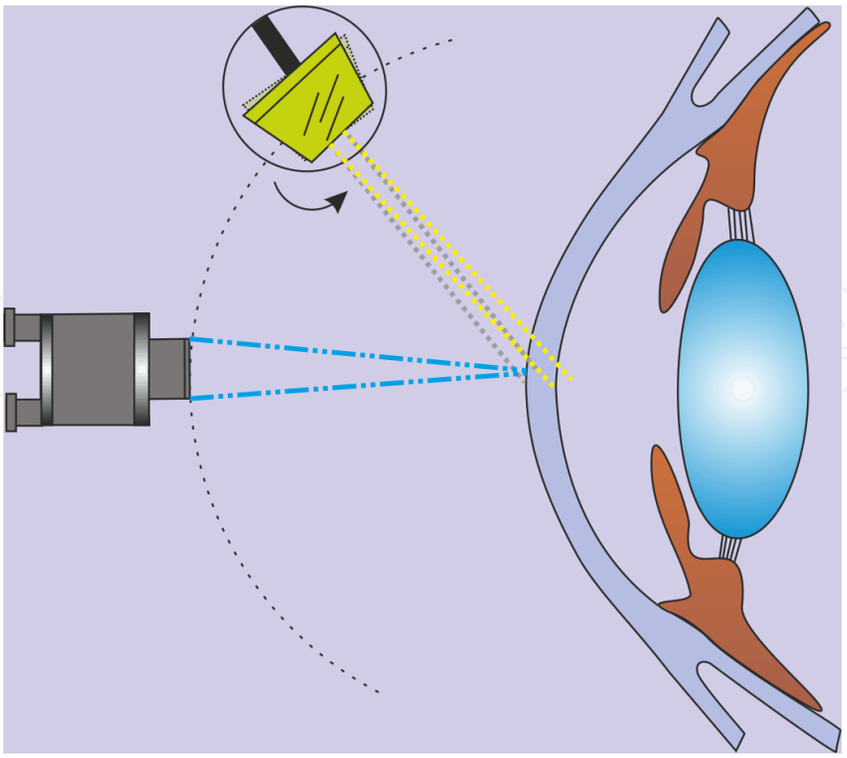

Figure 6. Indirect illumination

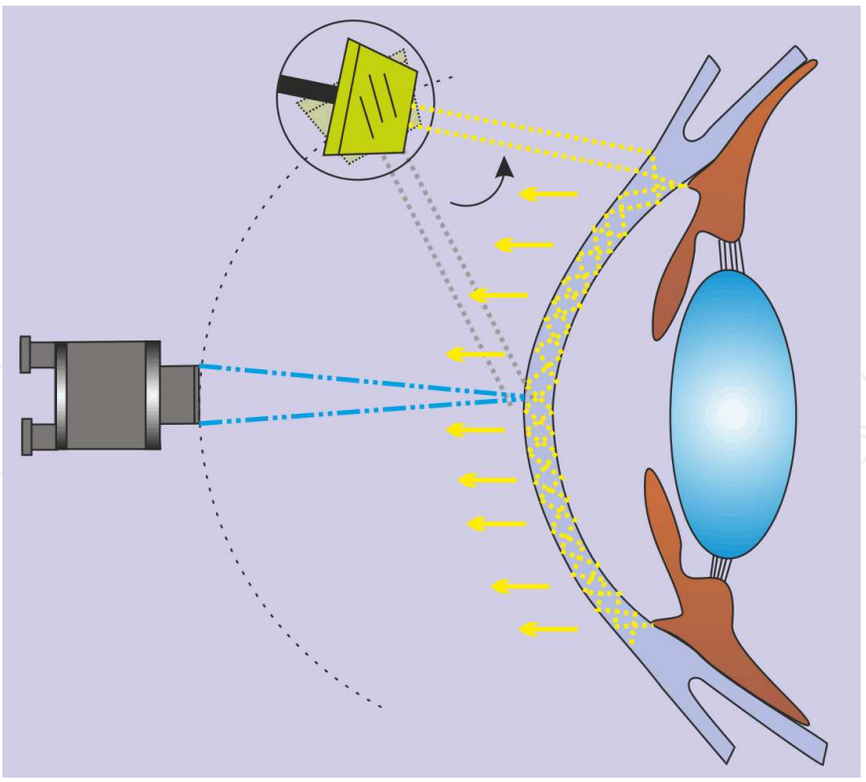

Figure 7. Indirect illumination, scleral scatter technique

Retro illumination can be used in visualization of central corneal opacities, lens and vitreous opacities, iris defects and pigment liberation. Procedure of the retro illumination is started with releasing of the knob. Angle between illumination and observing system should be set about zero. Then illumination system is focused on the object which is intended to be observed. When the beam is projected through the edge of the pupil, the bright light reflex returning from the retina can be seen (Figure 8A). If the beam is projected to the iris, corneal opacities and any vascularisation in the cornea or iris can be viewed by the reflected light (Figure 8 B) [2].

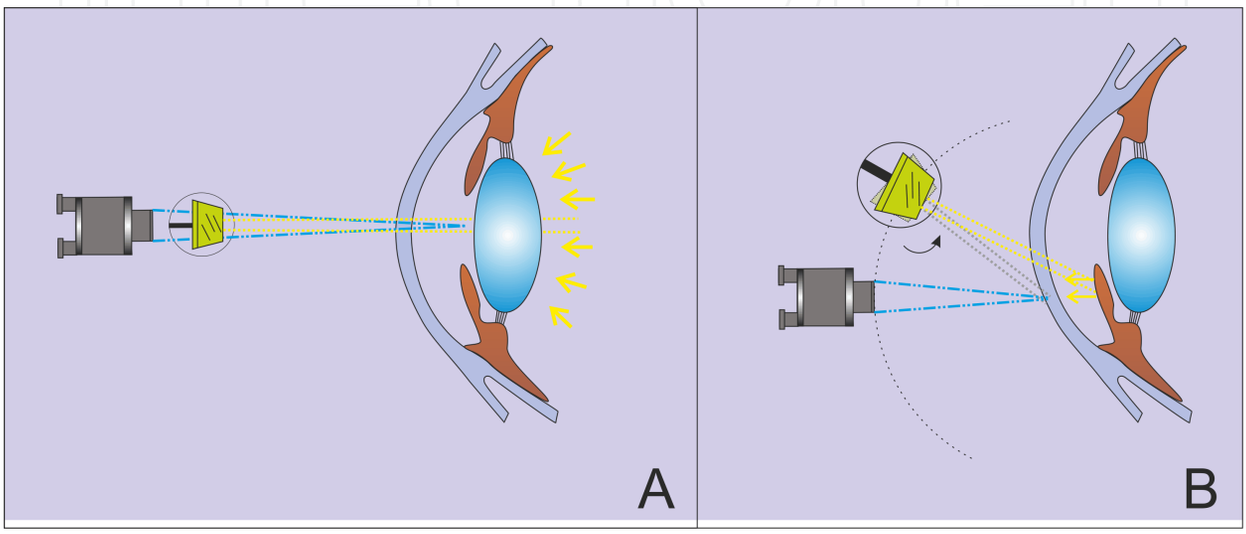

Figure 8. A. Fundus retro illumination. B. Iris retro illumination

2.2. Confocal microscopy

Confocal microscopy is a non-invasive histological imaging technique. It uses reflected light from the living tissue. Therefore, it is an in vivo imaging method of the living cornea. It uses focused light or laser beam. A bright light beam is projected and focused through an objective lens to the cornea. Then reflected light spot is collected from the illuminated tissue area by objective lens. With the help of beam splitter, reflected light is separated from the light mixture and directed to the detection unit. Reflected light reaches to the detection apparatus by passing a pin-hole. Detector transcodes the reflected light into electrical signal and records to the storage media (Figure 9). The pin-hole at the entrance of detector apparatus filters the light coming from outside the intended focal point. This filtration helps grabbing sharper and clearer images than conventional light microscopy [3].

For two-dimensional imaging, the sample is scanned sequentially in different focal planes. There are three types of confocal imaging techniques.

a. *Tandemn scanning confocal microscopy* was developed by Petran and Hadravsky [4]. Basic part of the system is the real time point illumination and point detection. It was developed by Nipkow in 1884 [5]. System provides real-time images at true color and marginal image quality based on the low intensity of reflected light [6]. Future development in tandemn

http://dx.doi.org/10.5772/58314

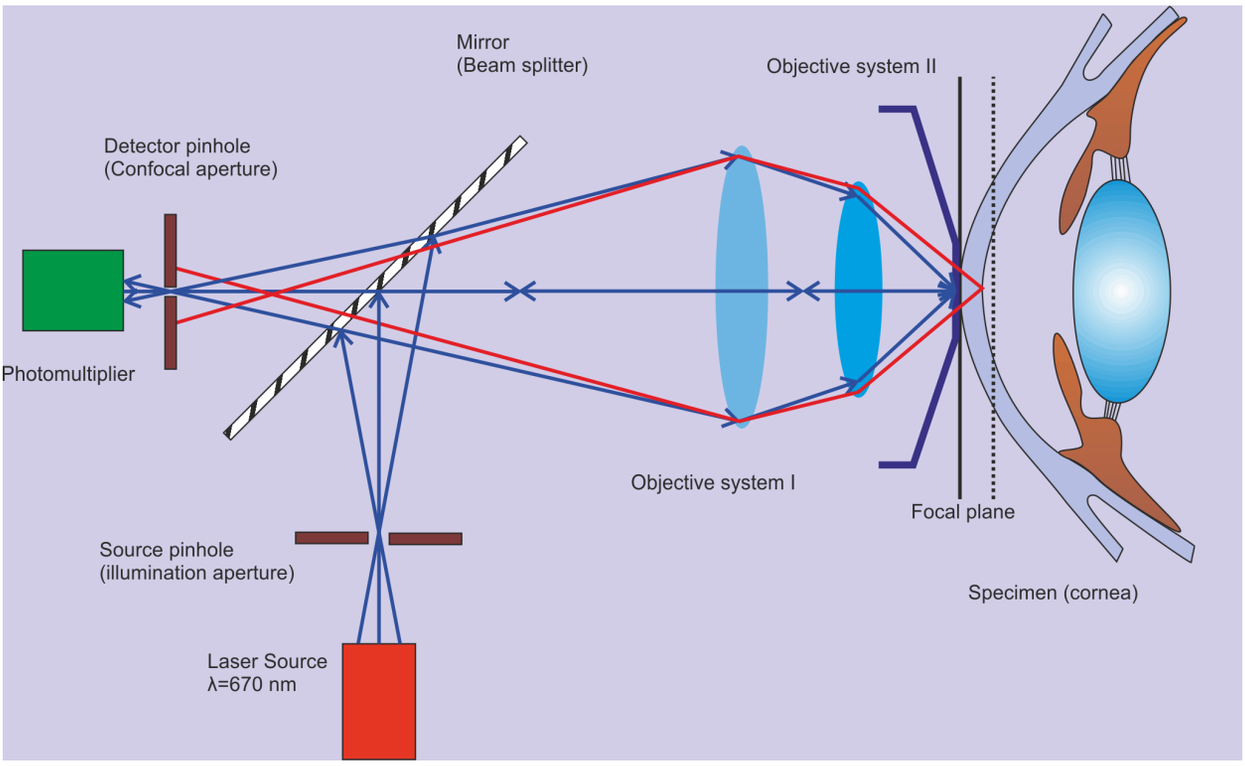

Figure 9. Working principle of confocal microscopy.

scanning was done by Xiao et al [7]. They used set of pin-holes on the same side of Nipkow disk for illumination and detection. The pinholes need to be as small as possible to eliminate the scattered light [4]. Design was simple but it has disadvantage of low intensity of illumination for image formation. Clinical version was produced but no longer in production [3].

b. *Scanning slit confocal microscopy* is an alternative scanning method to point scanning which uses a slit illumination. It scans over the back focal plane of the microscope. Advantage of slit scanning is that many points on the axis of the slit are scanned at the same time and therefore scanning time is markedly decreased. Scanning slit systems also have superior light brightness compared to point scanning. In comparison to pin-hole systems, slit scanning systems have lower axial and transverse resolution. Slit height, width and amount of light can be adjusted in slit scanning systems. By this way, visualization quality and optic section area can be modified based on the specimen i.e. transparent or opaque specimens.

c. *Laser scanning confocal microscopy* was developed by Webb in 1987 [8-10]. A coherent laser beam is used as a light source and specimen scanned by laser beam with the help of galvanometer scanning mirrors which provides fast scanning. Reflected light is refocused and projected to the photomultiplier through the pin-hole aperture. Heidelberg Retinal Tomograph is an example of in vivo confocal imaging systems. It uses 670 nm diode laser as a light source to acquire and analyze the optic nerve for glaucomatous damage. With the help of detachable optical attachment, HRT II was modified to high resolution confocal

laser scanning microscope by Stave et. al. [11]. It is named as 'Rostock Cornea Module'. High-contrast, high quality images of the cornea are produced by HRT III.

Clinical applications of confocal microscopy: Qualitative properties of cornea can be documented such as corneal thickness measurement, depth of surgical interfaces, densities of stromal and endothelial cells, density or nerves and reflectance and scatter at various depths [12]. Reliable measurements highly depend on experienced technician and grabbing good quality images.

Corneal epithelium is comprised of superficial epithelial cells, wing cells and basal epithelial cells. The superficial epithelial cells are 40-50 μm in length and appear as polygonal shape, bright nucleus and surrounded by dark halo in confocal imaging [5, 13]. The wing cells appears in confocal images as bright cell borders, bright nucleus without dark oval ring [14]. Basal epithelial cells are smaller (8-10 μm) than superficial cells and appears as regular mosaic of dark cell bodies with light, narrow intercellular borders [13]. Confocal microscopy allows clear in vivo visualization of the sub-basal nerve plexus running parallel to the corneal surface. Nerve plexus appears as bright well-defined linear structures, frequently demonstrating branches or anastomoses. Bowman's layer is identified in confocal microscopy as amorphous layer [15]. Corneal stroma can be clearly imaged with confocal imaging and good correlation has been reported between in vivo and ex vivo cell density [16, 17]. Stromal keratocytes are identified as hyperreflective cell nuclei with poorly visualized cell processes. Cell process may become more visible in corneal edema or trauma [15, 18]. Descement membrane appears as an acellular layer between posterior stroma and endothelium [15]. Confocal microscopy provides clear images of the corneal endothelium despite of moderate corneal edema [19]. Endothelial cells appear in confocal imaging as hexagonal shape cells with a honeycomb order [15].

The introduction of confocal microscopy into the research and clinical practice, represented a revolutionary approach to the inherited corneal diseases. It allowed the clinician in vivo microscopic analysis of affected corneas and screening of unaffected family members [20]. Besides the inherited corneal diseases, confocal microscopy can be used in determining the acanthamoeba keratitis, fungal keratitis, bacterial and viral keratitis [3, 21, 22]. Wound healing response can be analyzed after refractive surgery with confocal microscopy [3].

2.3. Scheimpflug imaging

The Scheimpflug principle, first described by Theodor Scheimpflug, a cartographer of the Austrian navy [23]. According to him, obliquely tilted object can be documented with maximal possible depth of focus and minimal image distortion. In a normal imaging camera, all planes are parallel to each other. But in a Scheimpflug imaging principle, all planes cuts each other in an intersection point (Figure 10). Scheimpflug principle was first introduced in ophthalmology by Drews, Niesel, Brown, Dragomirescu and Hockwin [24-27]. Scheimpflug imaging technique provides high resolution and wide depth-of-focused sharp images from anterior corneal surface to the posterior crystalline lens capsule. In this technique camera rotates along with a monochromatic slit light source around the optical axis of the eye to obtain slit images. This system scans the cornea from zero to 180° and each one of the photographs belongs to the

http://dx.doi.org/10.5772/58314

specific angle of corneal section (Figure 11). During the scanning process, a center placed static camera detects pupil contours and controls fixation.

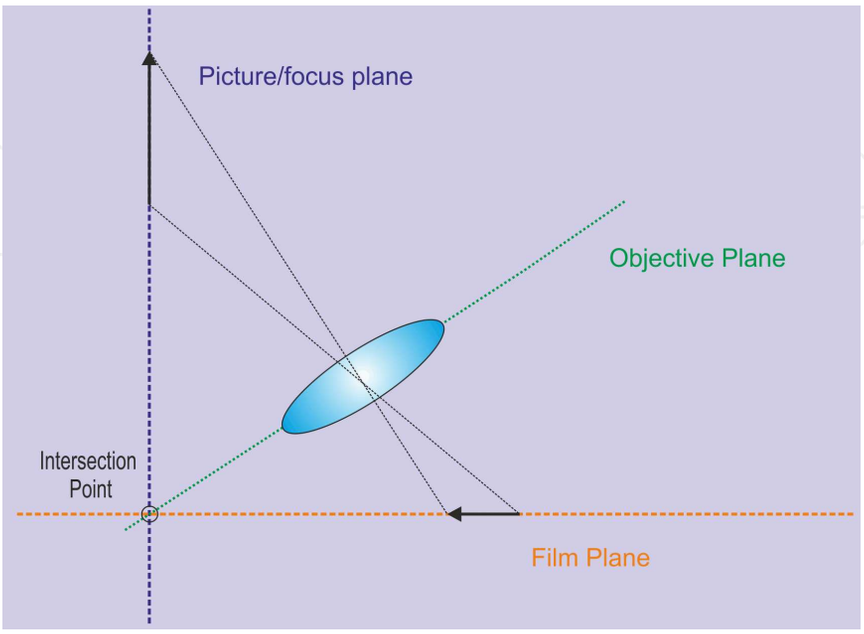

Figure 10. Scheimpflug principle imaging

Reconstruction of anterior and posterior corneal surface topography is done by analyzing of multiple photographs taken from specific angle. Corneal pachymetry, wavefront aberrations, densitometry of crystalline lens and anterior chamber calculations and measurements are provided by bundled software. Pentacam is a Scheimpflug imaging device available in market. There are three different model Pentacam versions available in the markets which are basic, classic and HR (high resolution). Differences between models are mostly in software but resolution upgrade is available in HR model [28].

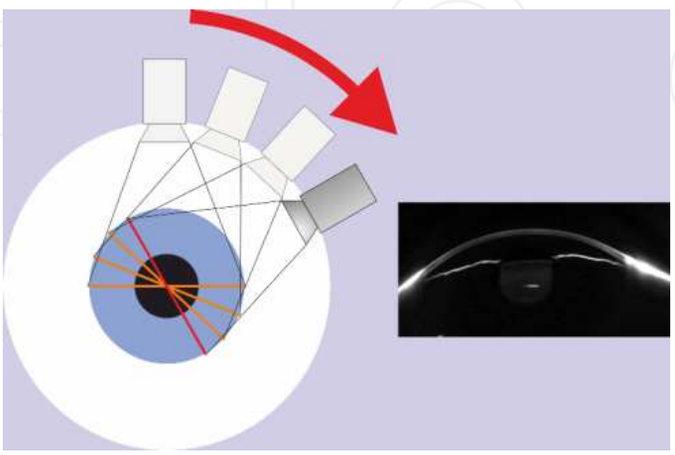

Figure 11. Scheimpflug photography technique

The other one is Galilei dual Scheimpflug analyzer which integrates a placido disc with a dual rotating Scheimpflug system [29]. Both systems acquire images simultaneously to obtain information on the curvature and elevation of the cornea. After scanning the anterior chamber, Scheimpflug images are transferred to PC to get analyzed and used to construct 3-D model of the anterior segment of the eye by the bundled software. Accuracy of the 3-D model increases with the count of the images and resolution of the camera. After constructing 3-D model, topographic and pachymetric measurements are done and entire anterior and posterior surfaces of the cornea are analyzed. Remodeled anterior chamber can be analyzed and viewed in any direction.

Basic software allows qualitative assessment of the cornea such as topography and elevation data of anterior and posterior corneal surface and pachymetry map. Topography maps are used for keratoconus detection, pre-surgical planning of refractive surgery, intra ocular lens (IOL) power calculation and follow-up after corneal and refractive surgery. Pachymetry maps allow representation of corneal thickness in color which covers from limbus to limbus. Measured values can be displayed and represented manually at any point. Corneal wavefront Zernike analysis can be performed by the software. 3-D anterior chamber analysis is used for pre-surgical planning of implantation of phakic IOLs, pre-post operative comparison of changes in anterior chamber, glaucoma screening, pachymetry-based IOP correction, assessment of anterior chamber volume, angle and volume.

Optional software modules such as Holladay Report, Holladay EKR Detail Report, Belin/Ambrosio Enhanced Ectasia Display, Contact Lens Fitting, 3D Posterior chamber IOL Simulation Software and 3D cataract analysis can be installed. The Holladay Report was developed by Jack T. Holladay, M.D [30]. It calculates the real relationship of the posterior corneal surface to the anterior corneal surface and provides data for calculating the optimal IOL refractive power for patients who have undergone refractive corneal surgeries. The Belin/Ambrosio display is the first keratoconus screening tool. It provides height data of the anterior and posterior corneal surface in combination with a progression analysis of the corneal thickness. It was developed by Michael W. Belin, M.D. and Renato Ambrosio Jr., M.D [31]. This module is used to early detection of keratoconus. Contact Lens Fitting module allows automatic display of all necessary measurement data for fitting contact lenses, automatic suggestions for contact lenses and realistic image simulation.

2.4. Anterior Segment Optic Coherence Tomography (AS-OCT)

Optical coherence tomography (OCT) is a non-contact imaging method which provides detailed cross-sectional images of biological tissues. It works with similar principle with ultrasound imaging. Delay time of reflected light is measured and used to visualize the target tissue in depth. A beam of infrared light is used instead of sound wave. Light travels extremely faster than sound wave and therefore measuring the delay time of infrared light is impossible. To overcome this limitation, delay time of light is measured by comparing the sample reflected light with a reference reflected light in an interferometer.

Resolution of OCT depends on the coherence length of the light and ranges from 2 μm to 20μm. High resolution capability and transparent structure of the anterior segment makes OCT an

ideal imaging technology. High frequency ultrasound of anterior segment and confocal microscopy also can reach similar resolution but OCT is more practical, non-contact, and faster.

OCT was invented by David Huang and colleagues in 1991 [32]. Joseph Izatt described anterior segment OCT in 1994 [32, 33]. First anterior segment OCT was based on time domain technique and used 1310 nm wavelength infrared light. Time domain technique requires mechanical movement of a mirror to estimate the latency of every axial scan (A scan) in the projecting light. Wavelength of light that is used in this technique limits the resolution to 18 μm and the mechanical part limits the speed of A-scans performed by the device to 2000 scan/sec [34].

With the invention of spectral domain OCT (SD-OCT), axial resolution is increased to 5μm and the A-scan speed to about 26000 – 40000 (depends upon manufacturer) per second with the 840 nm light and without a movable mechanical part. In SD-OCT, reference mirror is fixed and A-scan is produced by Fourier transformation of spectral interference patterns between the sample and reference reflections. SD-OCT can visualize bowman layer as a parallel line, thickness profile of epithelial and stromal layer separately. However, time-domain OCT cannot easily visualize epithelial layer and stromal layer separately. Time-domain OCT still has advantage of visualizing deep tissue structures and anterior chamber biometry [34].

Newest technology for AS-OCT is Swept-Source OCT (SS-OCT). It uses 1310 nm infrared light source and categorized as fourier-domain OCT. SS-OCT makes possible to reconstruct the three dimensional images of the anterior segment of the eye more accurately [35]. SS-OCT has 10μm vertical resolution and capable to make 300.000 A-scan in one second for 16 mm section. Scan width of SS-OCT is higher than SD-OCT (16mm versus us 6 mm) [34]. It is quite simple and less expensive than SD-OCT. SS-OCT based OCT device has been announced in the market recently.

AS-OCT enables objective evaluation of anterior chamber. It provides comparable data of anterior chamber depth and irido-corneal angle dimensions with ultra sound biomicroscopy (UBM) [36]. Specific dimensions of the iris and chamber angle provided by AS-OCT can be used in predicting the development of angle-closure glaucoma [37]. AS-OCT is also useful in evaluating anterior chamber anatomy and positioning filtering devices after glaucoma surgery [37]. Anterior chamber measurements provided by AS-OCT are also useful in pre-operative evaluation of keratorefractive surgery. Measurement of chamber depth is useful in sizing and predicting the postoperative position of phakic intraocular lenses to the corneal endothelium [38, 39]. AS-OCT produced pachymetry map helps preoperative prediction of keratoconus and postoperative evaluation of ectasia and corneal thinning [40]. It is also useful in analysis of corneal wound structure after refractive surgery. AS-OCT is also useful in placement of intracorneal ring segments. It can identify incision depth and intrastromal position of the ring segments precisely. Assessment of segment position may help physician to avoid depth related complications [41].

AS-OCT can provide useful information before and after corneal surgery including corneal transplants. In preoperative setting, it is useful for evaluation of graft donor tissue for thickness and structural preservation [42]. After descement stripping endothelial keratoplasty, it detects posterior lamellar dislocation, primary graft failure and anterior chamber crowding with

consequent chamber angle encroachment, possible descement membrane detachment and pupillary block [43]. It can successfully detect descement membrane detachment in case of corneal edema after corneal transplant or cataract extraction [44].

Beyond the surgeries, AS-OCT is a valuable tool in determining the hereditary or infective corneal pathologies. AS-OCT can visualize the full-thickness intrastromal deposits, and confirm the pattern and the depth of these intrastromal infiltrates in granular corneal dystrophy Type 2 [45]. It is ideal for evaluating the depth of injury due to a foreign body, laceration or ocular burn [46]. In microbial keratitis, AS-OCT can illustrate corneal infiltrates as hyperreflective areas [47].

2.5. Ultrasound biomicroscopy (UBM)

Ultrasound biomicroscopy allows in vivo detailed assessment of anterior segment structures even if an optical opacity is presented. UBM was developed by Pavlin, Sherar and Foster [48]. It is based on 50-100 MHz transducers which are incorporated into a B mode clinical scanner [48-50]. Similar with other imaging techniques, penetration decreases but, resolution increases with the increasing frequency. It requires supine positioning of the patient and ocular contact with a coupling gel or fluid bath. One percent methyl cellulose is used for fluid bath but saline can also be used. During the examination, transducer moves continuously. Careful attention must be paid not to contact the transducer with the eye during the examination, otherwise corneal abrasion may occur. Most of the commercially available devices provide 25μm axial resolution and 50μm lateral resolution. Tissue penetrations of these devices are approximately 4-5 mm [51]. Scanning procedure can be viewed in real time and recorded on media. Qualitative measurements can be done with using electronic calipers of bundled software. UBM device can record the B-mode images to the media and software can reconstruct 3D anatomy model of the scanned area. The images can be viewed in any direction after examination. UBM also can be used for ocular biometry to calculate IOL power but popularity has reduced due to be a invasive technique and commercialization of partial coherent interferometry technique which is non-invasive.

UBM systems are also suitable for imaging other parts of the eye. With the eye movement, conjunctiva, underlying sclera and even peripheral retina can be examined. It can provide diagnostic images for corneal diseases, glaucoma, cysts, tumors and lens implants. Anterior chamber depth can easily be measured with UBM. Corneal layers can be identified in cross section. The first highly reflective layer is corneal epithelium. Under the epithelium, bowman layer also can be differentiated as a highly reflective layer. Corneal stroma reveals low reflectivity under the bowman layer. Endothelium cannot be differentiated from descement membrane by UBM, but both can be seen as a highly reflective layer at the posterior corneal margin [52]. Corneoscleral junction and scleral spur can be distinguished. Trabecular meshwork cannot be visualized with UBM but identification of scleral spur locates its posterior extent. Iris epithelium forms as highly reflective layer on the posterior iris surface. This layer is useful in determining the interaction of intra-irideal lesions from lesions behind the iris [52].

UBM provides valuable information about anterior segment related diseases. It allows classification of angle closure glaucoma based on their anatomic differences [53]. It can help

to understand the mechanisms of angle closure glaucoma, pigmentary glaucoma, malignant glaucoma and other glaucoma types [53-55]. It can also help defining the mechanisms and results of various types of glaucoma surgery [56]. UBM appearance of filtration bleb is characterized by a fluid tract from the anterior chamber through the internal ostium, beneath the scleral flap and into the subconjunctival space. Low internal reflectivity is a sign of better IOP control. Location of accurate obstruction site of fluid flow can be determined by UBM imaging [51].

UBM can visualize patients with opaque corneas before making decision for corneal transplantation [57]. Depth of anterior chamber, state of the angle presence of synechiae and position of intraocular lens can be determined before surgery [52]. UBM is also useful in scleral diseases. It can differentiate extra-scleral and intra-scleral diseases and degree of scleral thinning [58].

In case of traumatic hypotony, UBM can detect cyclodialysis cleft even in the presence of anterior chamber swallowing [59]. After trauma, other causes of hypotony such as occult wound leakage, ciliary body membranes can also be detected. UBM can show the anterior chamber traumatic opacities and can detect small foreign bodies [60, 61]. UBM can provide valuable information in the management of anterior segment tumors [62].

3. Posterior segment and orbital imaging system

3.1. Fundus camera

Fundus camera is a specially designed low power microscope. It can take photo from surface to the posterior pole of the eye with an attached camera. It is used for imaging the eye, monitoring progression of a disease and screening purposes. With the retinal angiograph attachment, it can be used for diagnostic purposes. Most of the commercially available fundus cameras have 30-50 degrees view angle with magnification of 2.5x. Most of them have some modifications which allow visualizing 5x magnified view of 15 degree central retinal area. With the wide angle lenses, 140 degree retinal area can be visualized which minifies the image by half.

Fundus camera uses flash bulb as a light source. The light follows different paths in both observation and illumination systems. Observation light is focused via a series of lenses through a doughnut shaped aperture. When passing distance between the camera objective and corneal surface, it forms an annulus through central aperture. Reflected light coming back from the retina passes through the unilluminated hole in the doughnut formation [63]. Independent light travelling system minimizes the reflections of light source in the captured image. Retinal image projected through a low powered telescopic eye-piece allows selecting and focusing the retinal image. When the capture button is pressed, a mirror interrupts the illumination system and allows flash bulb light. Simultaneously, another mirror falls in front of the observation system which redirects the retinal image to the CCD camera. New devices use infrared light instead of a visible light to observe the retina to improve patient comfort, minimize reflections and to take undilated fundus images. Once the images have been captured, they are transferred to a connected PC for observation and analysis.

Bundled software's are capable of creating panoramic images of retina with processing multiple images taken from different areas of retina. Most of the fundus cameras have internal fixation point or external fixation point for taking images from different regions of retina and patient cooperation.

Digital SLR (single-lens-reflex) cameras provide superior image quality. They also require less illumination to capture photographs. This means less flash light requirement and better patient comfort. Recent devices combine digital SLR devices with fundus cameras to take digitally editable, high quality images. Capability of fundus camera instruments varies by model and manufacturer. They can perform color fundus photography, stereo fundus photography, red-free imaging, autoflourescence imaging and angiography of retina. Stereo fundus photography permits clinician to view the patient's fundus pathology in three dimensional from the print-out or computer screen.

In Recent years, usage of scanning laser technology in imaging of the posterior segment also allowed fast and wide field retinal image capturing. For example P200 (Optos PLC, Dunferline, Scotland) ultra-wide field non-contact retinal imaging camera uses red and green laser to scan the retina. It can produce up to 200 degree of high resolution retinal images in a single capture. It can also capture autofluorescence and fluorescein angiography images with additional modules [64].

Fundus photographs are visual records of the current opthalmoscopic appearance of a patient's retina. They allow the physician to identify retinal changes on follow-up or share the patient's condition with colleagues. It is mostly used for follow-up of glaucoma and diabetic retinopathy. Glaucoma is a condition which damages optic nerve over time. Physician can identify subtle changes in the optic nerve with serial fundus photographs and can recommend appropriate therapy to the patient.

It can document macular edema, newly occurred micro aneurysms and neovascularisation clearly. Detecting the macular edema may be easier with stereo fundus photographs..

3.2. Fundus Fluorescein Angiography (FFA)

FFA changed the diagnosis of macular and choroidal pathologic lesions in a revolutionary way. Although retina can be examined by slit lamp biomicroscopy, FFA provides valuable additive information to the practitioner. Fluorescein dye was first synthesized by Adolf von Baeryer in 1871 [65]. However, it was used as a diagnostic tool in 1960s by MacLean and Maumenee [66]. Modernization of fundus camera features, invention of special camera filters, improved optics, high resolution digital cameras and better understanding of biologic properties of fluorescein have changed FFA to a sophisticated valuable diagnostic tool in ophthalmology.

Fluorescein is used in ophthalmology as hydrocarbon salt of sodium with molecular formula $C_{20}H_{10}O_5Na_2$ (Figure 12) [67]. Molecular weight of fluorescein is 376.67 daltons and it is highly water soluble. Fluorescein has the ability to give off longer wavelength light after being exposed to a specific wavelength light. Excitation wavelength is 465 to 490 nm and fluorescence wavelength is 520-530 nm [68].

Figure 12. Marked form and chemical structure of sodium fluorescein.

Molecular weight is too large to pass through the RPE cells to pass through the RPE cells (Outer blood-retina barrier) and large choroidal vessels. But it is small enough to diffuse easily through the capillaries except central nervous system and retina (inner blood retina barrier) and these features makes it ideal for visualizing vessels [69]. Special feature for diagnostic purposes in ophthalmology is able to leak from disrupted blood-retina barrier areas. After injecting the fluorescein from antecubital vein, 80-85% of fluorescein binds to plasma proteins especially albumin [67, 69]. Unlike bound fluorescein, free fluorescein is able to absorb and emit light. Fluorescein is eliminated by glomerular filtration in the kidney and metabolized by liver [70].

The risks of angiography have been well described in literature [70, 71]. Mild reactions due to fluorescein angiograph are nausea, emesis, pruritus and vasovagal symptoms. The incidence of these reactions can be as low as 0,6% or as high as 15% [67, 69]. Most of the adverse effects are rapidly onset after injection and normally resolves approximately in 1,5 hours [71]. Severe reactions such as laryngeal edema, broncho spasm, anaphylaxis, shock, myocardial infarction, cardiac arrest and convulsion can be seen [72]. These reactions may even be fatal (1 in 222,000) [73]. Absolute contraindications include first trimester of pregnancy [74]. Relative contraindications are second and third trimesters of pregnancy, congestive cardiac, renal and hepatic failures [69].

After administration of fluorescein several phases can be seen in retinal circulation. Understanding the normal phases is essential for correct interpretation of FFA. These phases of FFA are shown in Figure 13. After administration of dye, fluorescence can be visualized in optic nerve and choroid within 10-15 seconds. But this interval can be changed by many factors such as injection site and circulation speed [75].

After initial appearance of dye in the choroid, arterial filling occurs 1-3 seconds later. Complete filling of arteries should finish less than 1 second. Venous filling phase occurs slower than arterial phase. Laminar filling of veins with dye can be seen in all individuals 2-3 seconds after completion of arterial filling (arterio-venous phase). It is named as also laminar venous filling. Venous filling should be completed in 11 seconds after first appearing the dye in arteries (Venous phase). Recirculation phase starts at 30th second after injection of dye and lasts approximately 2 minutes. In this phase, vessels are filled for the second cycle. With the

elimination of dye through the glomerular filtration, concentration of the dye in the blood stream declines during the recirculation phase. In the late phase of angiogram, no dye should be detected in the vessels. Fluorescence can be detected in the vessels in case of vascular leakage secondary to inflammation [75].

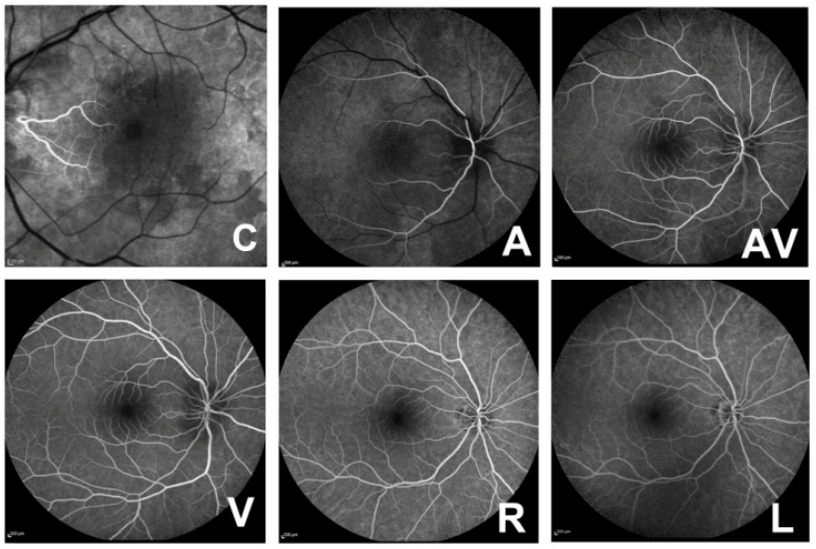

Figure 13. Phases of fluorescence angiography. C. Choroidal, A. Arterial, AV.Arteriovenous, V.Venous, R. Recirculation, L. Late phase.

Hypofluoresence can be detected in the FFA secondary to filling defects or blockage of fluorescence by an opaque medium. Filling defects can be seen by occlusion of small vessels in diabetes, radiation retinopathy, sickle cell disease or talc retinopathy. Capillary filling defects can be seen in diabetes and retinal vein and artery occlusion and Behcet's disease. Retinal arterial occlusion is observed as hypofluoresence in the retinal area distal to the site of the occlusion (Figure 15, A-B) [75].

Hyperfluorescence can be observed in 4 circumstances; leakage, staining, pooling and window defect. Window defect implies partial or total loss of blocking effect of RPE. It can be seen in geographic atrophy in macular degeneration and tear of the RPE. Neovascularisation in diabetic retinopathy, sickle cell retinopathy and choroidal neovascular membrane in AMD or myopic degeneration leads to leaking appearance. Microaneurysms in diabetes, Irvine-Gass syndrome, uveitis induced macular edema and arterial macroaneurysms are example of leakage due to the permeability loss of vessels [75]. Pooling means accumulation of the dye in fluid filled spaces. Examples of pooling appearance are central serous chorioretinopathy, pigment epithelial tear in AMD and intra ocular tumors. Staining is increased intensity of hyperfluorescence in a lesion. Examples of staining are disciform scars, regressed neovascular tissue, myopic degeneration and gyrate atrophy (Figure 14, C-F).

http://dx.doi.org/10.5772/58314

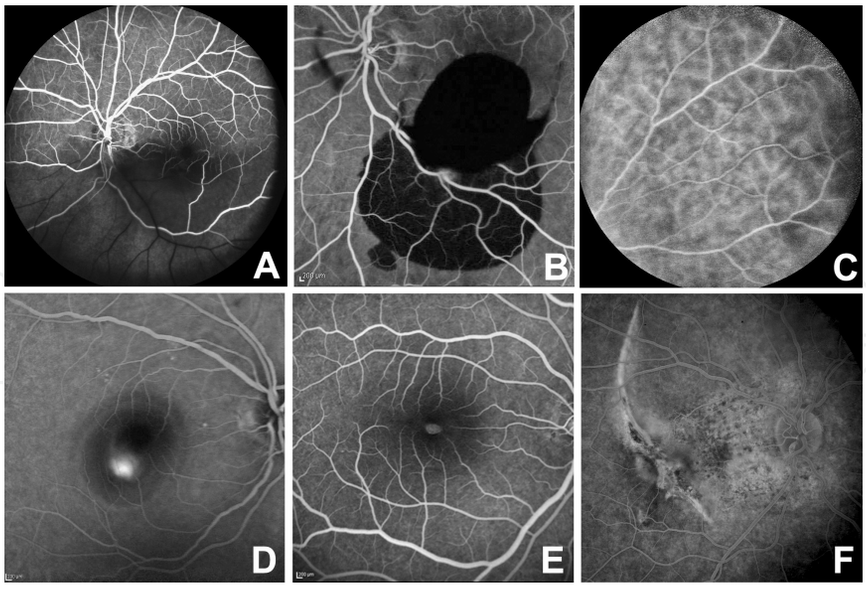

Figure 14. Sample FFA images A. Filling defect due to the occlusion of major artery, B. Blockage of fluorescence in intravitreal hemorrhage C. Leakage in behcet uveitis. D. Pooling in SSR, E. Window defect in macular hole, F. Late staining in choroidal scar.

3.3. Indocyanine green angiography

Investigations for visualizing the choroidal vasculature introduced the indocyanine green (ICG) angiography into the ophthalmology. It was first introduced into medicine in 1957 for measuring the cardiac output [76, 77]. In 1986 Hayashi et. al improved new filter combinations with sufficient sensitivity [78]. Indocyanine green is a water soluble dye and molecular weight is 775 daltons. Molecular formula is C43H47N2NaO6S2 [79] (Figure 15). It absorbs near-infrared light the range of 790-805 nm. Emission spectrum is in the range of 770-880 nm, peak at 835 nm. Indocyanine green bounds to plasma proteins with 98% but unlike fluorescein, 80% of indocyanine green bounds to the globulins such as A1-lipoprotein [79]. Therefore indocyanine dye cannot escape from choroidal vasculature and allows visualizing of the choroidal vasculature. ICG diffuses through the choroidal stroma slowly and stains in the choroid during the 12 minutes after injection.

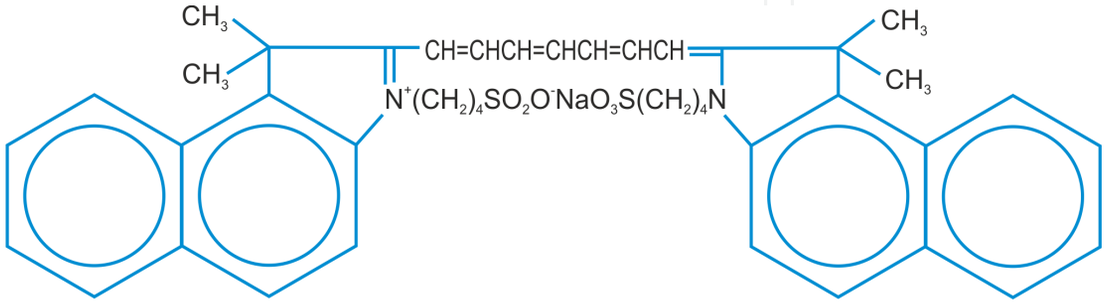

Figure 15. Molecular structure of indocyanine green

Standard dosage of ICG is 25 mg which is dissolved in 5 ml solvent. It should be injected rapidly through the antecubital vein. It is taken up by liver and secreted into the bile without metabolic alteration. It is a safer dye than fluorescein. Adverse reactions are rare. Nausea, vomiting and pruritus can be seen in 0.15% of patients. Isolated vasovagal type reactions and anaphylactic shock have been reported in the literature [80-82].

Image acquisition from ICG done by the near infrared laser or light through the excitation filter. Excited ICG molecules emits slightly different wavelength of light. Before being captured by the camera, emitted light passes the barrier filter which blocks the light with a shorter wavelength than 825 nm. Therefore, the camera captures only the light which is emitted by ICG, not the projected light near infrared spectrum [79].

Digital image capturing and processing systems made it easy to capture, view and store the acquired images. The Charge coupled device captures the ICG angiography images and converts to digital data. SLO systems provide high capturing sensitivity and allow simultaneous capturing with fluorescein angiography and ICG angiography. SLO systems use infrared diode laser (795 nm) to excite the ICG. The use of wide angle lenses allows instantaneous imaging of large fundus areas.

ICG angiography is widely used in the detection and follow-up of AMD related lesions. Serous pigment epithelial detachment is an ovoid or circular detachment of retina pigment epithelium and seen as blockage of normal choroidal vessels in ICG. Choroidal neovascularization (CNV) is a choroidal capillary proliferation through a break in the bruch membrane. Classic CNV can be detected as an area of bright hyperfluorescence but it can be better delineated by fluorescence angiography. Occult CNV without serous pigment epithelial detachment can be seen as early vascular hyperfluorescence and late staining of abnormal vessels. Occult CNV with serous pigment epithelial detachment reveals as early vascular hyperfluoresence and late staining of the CNV [83, 84]. Hot spot or focal CNV is seen as well delineated and no more than one disc diameter in size with ICG angiography.

Polipoidal choroidal vasculopathy is an abnormality of the choroidal circulation. it is seen as distinct network of vessels in choroid at the early phases. Retinal angiomatous proliferation is characterized by dilated retinal vessels, retinal hemorrhages and exudates. In ICG, it reveals as focal areas of intense hyperfluorescence (hot spot) and late extension of leakage which corresponds to intraretinal neovascularization. Central serous chorioretinopathy is a collection of fluid under the retina and makes visual distortion. It is detected in ICG angiography as multifocal areas of hyperfluorescence in early and late phases. ICG angiography is a valuable diagnostic tool in the evaluation of intraocular tumors. Pigmented choroidal melanomas absorb and block ICG fluorescence. It can be used for differentiation of choroidal melanomas from non-pigmented intra ocular tumors [79].

ICG angiography also can provide valuable information about intraocular inflammatory conditions.

http://dx.doi.org/10.5772/58314

3.4. Scanning Laser Ophthalmoscope (SLO)

SLO is a tool which can be used for FFA, ICG angiography, autoflourescence detection and acquiring OCT images with modification. Combination of low powered laser illumination and confocal imaging technique provides high contrast and detailed images. Using very narrow and exact wavelength laser allows more efficient excitation than filtered flash illumination of the fundus camera. Due to the monochromatic laser, captured images are in gray scale.

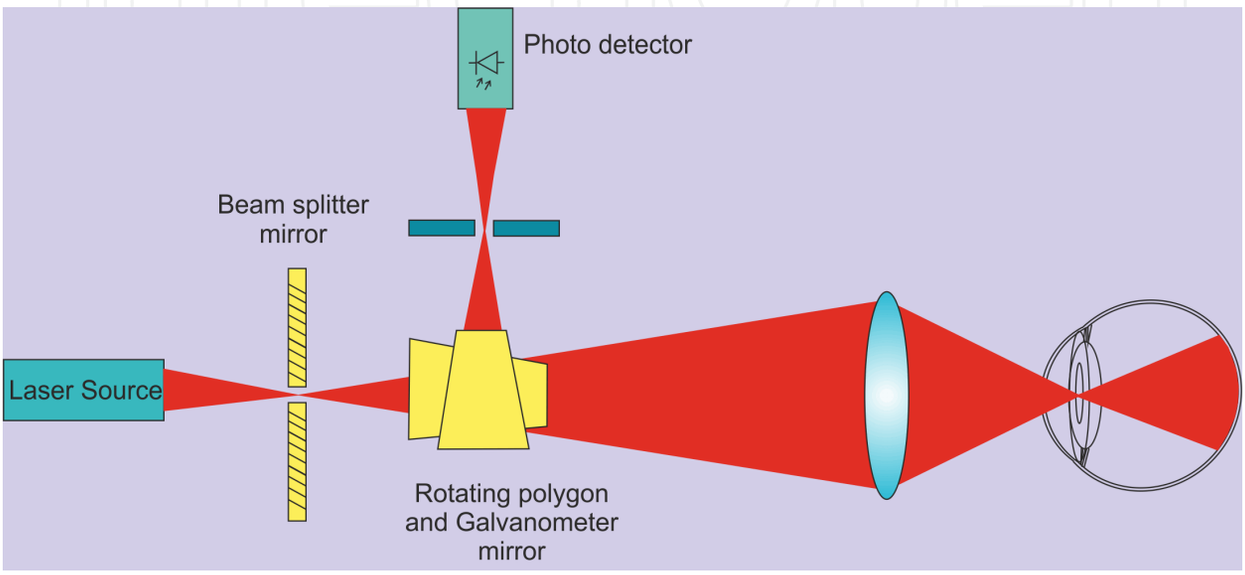

Figure 16. Working scheme of scanning laser opthalmoscope

SLO imaging principle basically starts with the pre-shaped laser beam which is focused to the retina. Pre-shaped laser beam passes through the 2mm aperture of a beam splitter mirror. Beam is deflected horizontally by a rotating polygon mirror to form a line scan. Galvanometric mirror is deflected vertically to form a two dimensional raster. Two dimensional raster laser beams are focused to a single point at the patient's lens which refocuses it onto the retina. The light reflected from the retina travels the same path and rescanned by two scanning mirrors. Beam separator collects the reflected light and focuses it onto the photo detector (Figure 16). Photo detector converts the reflected light to the images and transmits to the computer for processing and recording. Advantage of SLO is reduced scattered light in the reflected light. Reduced scattered light results with improved image contrast.

There are two types of SLO-based device available in the market. These are Heidelberg Retinal Tomography (HRT) and Heidelberg Retinal Angiography (HRA). HRT is designed to acquire images from especially optic nerve and macula. It provides quantitative three dimensional imaging of the posterior segment. HRA uses 670nm laser diode and confocal aperture to acquire images. HRT II has 15-degree scan area. Image resolution is 384x384 pixels. Scan depth ranges between 1 to 4 mm. Sixteen images are captured at each 1 mm. After acquiring images, bundled software allows the analysis of retinal thickness and optic nerve topography [85].

HRA is a confocal SLO designed for simultaneous FA, ICG angiography and autoflourescence imaging. Blue laser (488nm) is used for exciting fluorescein and near infrared laser (795nm) is used for exciting indocyanine green dye. Barriers for acquiring emitted light are 500nm for FA and 810nm for ICG angiography. The field of range starts from 10°x10° to as much as 150°x 150° with the contact lens attachment [86]. Another firm 'Optos' also combined the scanning laser ophthalmoscope with OCT [87].

3.5. Optical Coherence Tomography (OCT)

Transparent structure of the eye allows us visualizing the fundus non-invasively. OCT also provides cross sectional and high resolution images of retina, retina nerve fiber layer, optic nerve and choroid non-invasively. Beyond the posterior segment, anterior segment OCT devices also present and can provide images of cornea, lens, iris and angle structures. Spectral domain (SD) technique provides 5-7μm axial resolution which means an in-vivo optical biopsy of the retina. OCT uses super luminescent diode to obtain a coherent laser beam for imaging the retina. Reflected and scattered light beam from the vitreoretinal interface, layers of the retina and choroid allows acquisition of images. There are two basic technique present for OCT imaging; time-domain and spectral domain techniques.

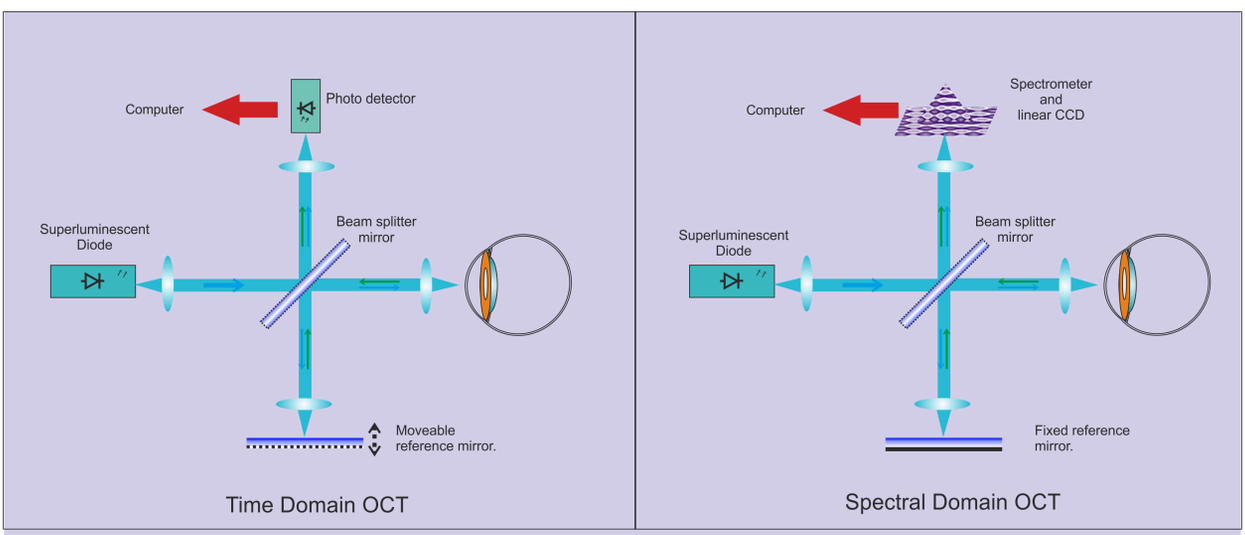

Figure 17. Comparison of time domain and spectral domain OCT working principle

Time-domain technique emits laser beam by super luminescent diode. The beam is splitted into two different paths by a beam splitter. First beam is sent to ocular media, other beam is sent to the movable mirror. Reflected light from the ocular media and movable mirror are combined on the same path and a partial interference is created. Photo detector and the computer measure the interference amplitude and calculate the depth information for each A-scan. To create a B scan image, A-scan sequences are repeated for different directions. Obtained image quality depends on the count of A-scan in each direction (Vertical, horizontal, oblique) and absorption rate of the projected light by tissue. Time-domain devices can provide 400 A

scans per second with a maximal axial resolution of 8-10μm (Figure 17). High quality images require longer time to create. Therefore time is the major limitation of this technique. Time-domain technique cannot visualize deeper layers such as choroid due to the light scattering feature of the RPE and low signal-noise ratio [88](Figure 18 A).

In SD-technique, the light source is the same as in time-domain technique. There is also a reference mirror, but it is fixed unlike time-domain technique. This technique uses spectrometer and linear CCD for analyzing interferences between sample beam and reference beam. Fourier transform equation is used for calculating interference information. Absence of movable mirror speeds up the image acquisition up to 50 times. This technique enables to obtain large numbers of A-scans that allows creating high resolution images. SD devices can provide 20.000-52.000 A-scan per second with a 5-7μm resolution [89](Figure 18 B). Such a speed reduces the eye movement artifacts. Obtaining large numbers of images in a short period of time allows 3D reconstruction of the examined area.

One of the newer techniques in OCT imaging modalities is swept-source OCT (SS-OCT). It uses a different form of fourier analysis and employs tunable frequency swept laser source. Unlike spectral OCT measurements, interference is detected with photo detectors instead of spectrometer. Axial scan rate of SS-OCT is 100.000 to 236.000 per second with 11μm tissue resolution [90-92]. Prototype OCT systems using longer wavelength light are also present. Using longer wavelength light provides better penetration of deep tissues and allows visualizing of the choroid and opaque media in better detail [93]. Another new technology is Doppler OCT which detects the precise location of vascular abnormalities using cross sectional imaging. It can evaluate blood flow and volume of retinal and choroidal vasculature [94].

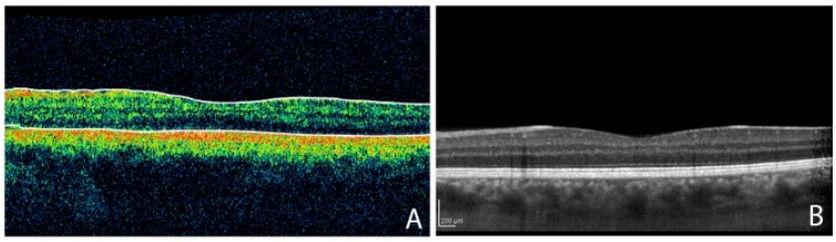

Figure 18. A. Macular cross-section acquired by time domain OCT, B. Macular cross-section image acquired by spectral-domain OCT

Automated retinal thickness measurements calculated by OCT devices are used for monitoring disease progression and response to therapies such as AMD, diabetic macular edema and vein occlusions. Accurate measurement of the retinal thickness helps physician for clinical decision regarding treatment in these conditions. Determining the retinal nerve fiber layer profile with OCT provides valuable information in detecting and management of glaucoma patients. OCT helps in diagnosing and classification of the macular holes. The determined size and configuration by OCT helps predicting the surgery outcomes [95, 96]. It allows evaluation of the vitreoretinal interface in epiretinal membrane and vitreoretinal traction [97]. OCT contributed to better understanding the AMD and helped monitoring the progression and therapeutic response to the intravitreal injections [98]. It is a valuable tool for early diagnosis, analysis and

monitoring of diabetic retinopathy with high repeatability and resolution [99]. OCT provides quantitative assessment of retinal thickness in diabetic retinopathy [100].

3.6. Ocular ultrasonography

Ultrasound is a safe, non-invasive, widely used diagnostic tool in medical imaging. It has an important role in ophthalmological diagnosis. Ultrasound produces two-dimensional cross-sectional views of the eye and orbit. It has especially important role for imaging intraocular lesions in the presence of anterior segment opacities. Ultrasound devices produce acoustic sound waves above the audible range of 20KHz to visualize ocular and orbital tissues. Acoustic sound is created by a piezoelectric crystal which is a transducer for converting electric energy into the ultrasound. A short acoustic wave generated by a piezoelectric crystal is sent to the examining tissue. Some of the ultrasound waves are reflected back to the probe. Probe converts returned echoes into electrical signal and image of the tissue is created with processing and combining every electrical signal (Figure 19).

Currently ophthalmic ultrasound devices use 8-100 MHz frequency echoes. In other fields 2-6 MHz frequency is mostly used. Higher frequencies provide increased resolution but decreased pentrance. Eye is a superficially located tissue and has low absorptive properties which make the use of high frequencies practical.

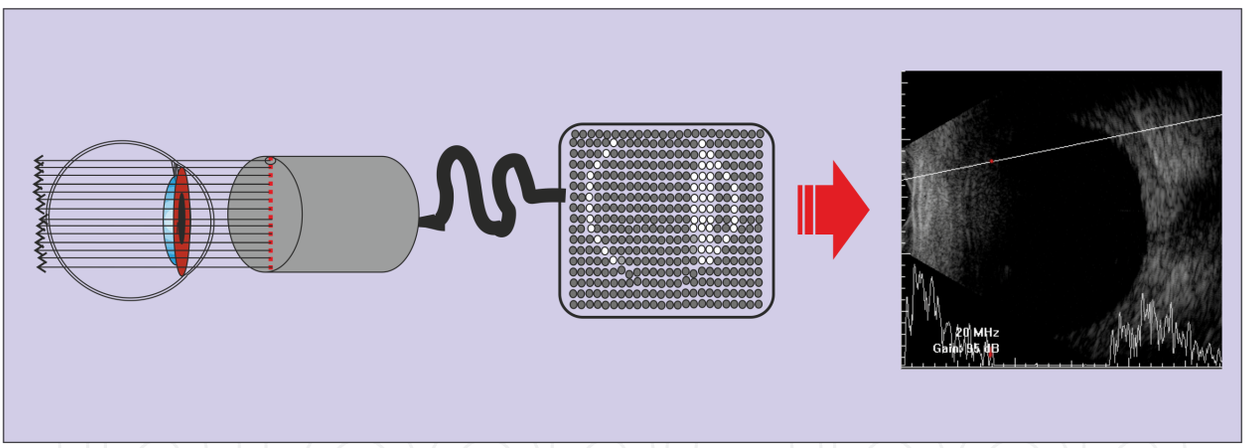

Figure 19. Working principle of ultrasonography

First report of ultrasound applied in ophthalmology belongs to Munth and Hughes who reported A-scan ultrasonography of intraocular tumors in 1956 [101]. B-scan images of the specific ocular diseases and tumors has been described two year later after the initial publication [102]. Most frequently used ultrasound imaging modes are A-scan, B-scan, ultrasound biomicroscopy, color doppler ultrasonography and three dimensional ultrasonography. Ultrasound biomicroscopy has been discussed in detail above.

Ocular ultrasonography is frequently used for evaluating intra ocular tissue integrity, searching and diagnosing intraocular foreign bodies, assessment of intraocular or peri-ocular lesions and examining trauma patients. It is frequently used in the presence of opaque media

such as cataract, corneal pathologies, etc. It can be used for determining intralesional characteristics or ecographic nature of a visible mass or foreign body.

A-scan imaging is a one dimensional display of echo strength over time. Vertical height corresponds to echo intensity. There are two types of A-scan present in opthalmological use; biometric A-scan and standardized diagnostic A-scan. Biometric A-scan is used for axial length measurement and corneal pachymetry in evaluation of ocular hypertension and calculation of intraocular lens power [103]. It uses 10-12 MHz frequency and has linear amplification curve. Standardized A-scan is used with 8MHz probe. It is used to determine and differentiate abnormal intraocular tissues. Retina consists highly dense ocular structures such as sclera and choroid which produces 100% echo spikes.

B-scan is the two dimensional view of the combined multiple A-scan echoes. Unlike A-scan, every spike is encoded as a bright dot and every dot brightness changes with the strength of the echo. B-scan images are highly accurate representations of ocular structures and provide shape, location and extensive information. Most of the ophthalmic ultrasound devices use 10MHz frequency for B-scan imaging. The evaluation and differentiation of intraocular lesions are one of the primary indications for ultrasonography. Combined use of B-scan and A-scan provides more reliable information for evaluating ocular lesions. Simultaneously viewing kinetic properties of echo amplitudes (A scan) with B-scan provides more accurate evaluation of intraocular lesions such as choroidal melanomas [104].

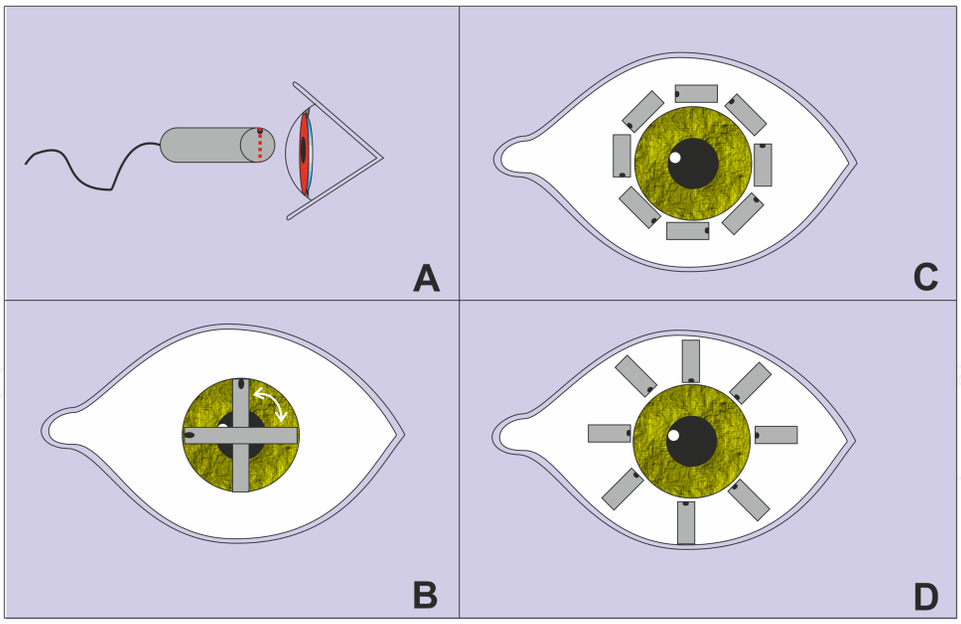

Figure 20. B-scan orientations A. External view of axial scan probe orientation B. Axial scan orientation, C. Transverse scan orientation, D. Longitudinal scan orientation

B-scan probe can be applied to the eye in axial, transverse and longitudinal orientation. Axial scan can be obtained by placing the probe across the visual axis through the cornea and lens. It is the easiest and mostly used orientation but sound attenuates due to the lens. This limits

its diagnostic use (Figure 20). Longitudinal scan can be obtained by placing the probe on sclera to visualize the specific clock hour anterior-posterior cross section. Transverse B-scan also can be obtained by placing the probe on the sclera parallel to the limbus. It provides antero-posterior dimension of the lesion. These two methods is not affected by the attenuation effect of the lens. It provides lateral dimension of the lesion.

Color-doppler ultrasonography allows evaluating B-scan image of the eye and blood flow simultaneously. If the flow moves toward the transducer it is coded with red color. The blood flow that moves away from the transducer is coded with blue color. It provides valuable information about vasculature of orbital tumors, carotid disease, central retinal artery and vein occlusions and non-arteritic ischemic optic neuropathy [105-107].

Ophthalmic 3D ultrasonography uses multiple consecutive two-dimensional B-scan images to create three-dimensional blocks with the help of bundled software. Specially designed transducer probe rapidly scans the eye in trans-scleral orientation and software creates the 3D image. It is useful for calculating the volume of the intraocular lesions [108].

3.7. Computerized Tomography (CT)

Computed tomography is a useful imaging tool in the evaluation of most orbital and ocular lesions. It allows us to detect location, extent and configuration of the lesion. It also provides tissue mass composition and helps planning of an appropriate surgical approach to minimize morbidity. Computed tomography works slightly different than conventional X-ray imaging methods. CT uses x-rays but it emits a thin collimated fan shaped beam. The beam is attenuated as it passes through the tissues and detected by array of special detectors. Detectors create electrical signals from attenuated X-rays and then signals are converted to the images.

CT provides images from thin slices of tissues and it is devoid of superimposition. Spatial resolution of CT scan depends on slice thickness. Thinner slices have higher resolution. Slice thickness of CT imaging can vary between 1-10 mm. Thin slices are good for ocular use but it requires higher radiation dose, greater number of slices and longer examination time. Therefore, slice thickness should be balanced based on the requirement of the case. Optimal slice thickness for eye and orbit is 2 mm [109]. CT requires less time and cheaper than magnetic resonance imaging (MRI). CT is superior in imaging bony structures and in the presence of blood. Therefore, it is excellent in trauma patients. Iodinated contrast agents are used for enhancement to detect intracranial extension of orbital tumors and to evaluate optic chiasmal lesions.

CT is indicated in unexplained propitosis, opthalmoplegia, pitosis, palpable orbital mass, preseptal cellulites, orbital trauma and orbital signs of paranasal sinus diseases. One should request CT imaging only when absolutely indicated because of X-ray exposure.

3.8. Magnetic Resonance Imaging (MRI)

MRI has complex working principle but it has one of the largest diagnostic potential in medicine. It is especially used for imaging neural tissue visualization and has substantial

advantage to other imaging methods. MRI creates images with the help of magnetic field and radio waves. It is based on the ability of a small number of protons within the body to absorb and emit radio wave energy when the body or tissue is exposed to strong magnetic field. Soft tissue contrast ratios of MRI are superior to other imaging modalities. Differences in the density of protons in different tissues are provides discriminating one from other. Different tissues absorb and release radio wave energy at different characteristic rates.

Various pulse sequence techniques are used in MRI imaging but most popular ones are T1 and T2-weighted images. T1 images measures ability of protons in a tissue to exchange energy with the surrounding environment or how fast the tissue is magnetized. T2 images measures how quickly the tissue loses its magnetization. In T1 images, fat appears as bright and water appears dark. Reverse view is present in T2 images. T1 images are used especially for viewing anatomy. T2 images are more valuable for detecting pathology. Contrast materials enhance recognition of primary pathology by demonstrating areas of breakdown of the blood-brain barrier.

MRI uses non-ionizing radiation. It can generate images through the entire body. It can visualize the tissue in sagittal, coronal and axial planes. It can visualize vascular tissues with or without contrast material. Beyond the advantages, it is relatively expensive and not widely available. Claustrophobia may be a problem for some patients. Cardiac pacemakers or implanted ferromagnetic foreign bodies are contraindications for MRI.

3.9. Angiography

There are three type of angiography imaging techniques. These are digital subtraction angiography, CT-angiography and MR-angiography. Digital subtraction angiography uses X-rays and iodine based intra-arterial contrast material. It subtracts the structures other than the vascular system, such as bone and muscles. It is still the gold standard method for imaging intra- and extra-cranial vasculature and in the diagnosis of cerebral aneurysms.

CT-angiography uses X rays and iodine based contrast agent. After bolus injection of the contrast agent from antecubital vein, high speed CT scan is performed. It provides images of three dimensional view of surface anatomy with color and blood vessel anatomy without color. It needs shorter examination times that MR-angiography and superior image resolution. Implanted magnetic foreign body is not a contraindication. It is safer and faster than digital subtraction angiography. It can outline surgical anatomy finer than MR-angiography.

No requirement of ionizing radiation and iodinated contrast agent are the main advantages of MR angiography over CT scan.

4. Conclusion

Imaging modalities has changed greatly in recent years. Especially newest OCT technologies promise better understanding and diagnosing of the disease. Advances in laser technologies and optical systems also have enhanced image quality and resolution in most of the imaging techniques. Newest digital technologies enable more easily reproducible information and

facilities telemedicine applications. Examination in Ophthalmology starts with imaging the eye either with inspection or a sophisticated tool. Caution should be taken no to skip the basic techniques and principles while evaluating the patients. Otherwise we can spend valuable time and money with sophisticated tests unnecessarily.

Author details

Umit Yolcu[1*], Omer Faruk Sahin[2] and Fatih C. Gundogan[3]

*Address all correspondence to: umit_yolcu@hotmail.com

1 Siirt Military Hospital, Ophthalmology, Siirt, Turkey

2 Etimesgut Military Hospital, Ophthalmology, Ankara, Turkey

3 GATA Medical School, Ophthalmology, Ankara, Turkey

References

[1] Nema HV, Nema N. Diagnostic Procedures in Ophthalmology. New Delhi2009.

[2] González J, Benavides C. Atlas of Slit Lamp: (ocular Biomicroscopy): Imagen y Comunicación Multimedia; 2004.

[3] Guthoff RF, Zhivov A, Stachs O. In vivo confocal microscopy, an inner vision of the cornea - a major review. Clinical & experimental ophthalmology. 2009;37(1):100-17.

[4] Petran M, Hadravsky M. Tandem scanning microscope--a new tool for three-dimensional microanatomy. Progress in clinical and biological research. 1989;295:551-8.

[5] Bohnke M, Masters BR. Confocal microscopy of the cornea. Progress in retinal and eye research. 1999;18(5):553-628.

[6] Bohnke M, Masters BR. Long-term contact lens wear induces a corneal degeneration with microdot deposits in the corneal stroma. Ophthalmology. 1997;104(11):1887-96.

[7] Xiao GQ CT, Kino GS. Real-time confocal scanning optical microscope. Applied Physics Letters. 1988;53(8):716–18.

[8] Davidovits P, Egger MD. Scanning laser microscope. Nature. 1969;223(5208):831.

[9] Davidovits P, Egger MD. Scanning laser microscope for biological investigations. Applied optics. 1971;10(7):1615-9.

[10] Webb RH, Hughes GW, Delori FC. Confocal scanning laser ophthalmoscope. Applied optics. 1987;26(8):1492-9.

[11] Stave J, Zinser G, Grummer G, Guthoff R. [Modified Heidelberg Retinal Tomograph HRT. Initial results of in vivo presentation of corneal structures]. Der Ophthalmologe : Zeitschrift der Deutschen Ophthalmologischen Gesellschaft. 2002;99(4):276-80.

[12] Erie JC, McLaren JW, Patel SV. Confocal microscopy in ophthalmology. American journal of ophthalmology. 2009;148(5):639-46.

[13] Jalbert I, Stapleton F, Papas E, Sweeney DF, Coroneo M. In vivo confocal microscopy of the human cornea. The British journal of ophthalmology. 2003;87(2):225-36.

[14] Masters BR, Thaer AA. In vivo human corneal confocal microscopy of identical fields of subepithelial nerve plexus, basal epithelial, and wing cells at different times. Microscopy research and technique. 1994;29(5):350-6.

[15] Mustonen RK, McDonald MB, Srivannaboon S, Tan AL, Doubrava MW, Kim CK. Normal human corneal cell populations evaluated by in vivo scanning slit confocal microscopy. Cornea. 1998;17(5):485-92.

[16] Patel S, McLaren J, Hodge D, Bourne W. Normal human keratocyte density and corneal thickness measurement by using confocal microscopy in vivo. Investigative ophthalmology & visual science. 2001;42(2):333-9.

[17] Patel SV, McLaren JW, Camp JJ, Nelson LR, Bourne WM. Automated quantification of keratocyte density by using confocal microscopy in vivo. Investigative ophthalmology & visual science. 1999;40(2):320-6.

[18] Vanathi M, Tandon R, Sharma N, Titiyal JS, Pandey RM, Vajpayee RB. In-vivo slit scanning confocal microscopy of normal corneas in Indian eyes. Indian journal of ophthalmology. 2003;51(3):225-30.

[19] Hara M, Morishige N, Chikama T, Nishida T. Comparison of confocal biomicroscopy and noncontact specular microscopy for evaluation of the corneal endothelium. Cornea. 2003;22(6):512-5.

[20] Vincent AL, Patel DV, McGhee CN. Inherited corneal disease: the evolving molecular, genetic and imaging revolution. Clinical & experimental ophthalmology. 2005;33(3):303-16.

[21] Zhivov A, Stachs O, Kraak R, Stave J, Guthoff RF. In vivo confocal microscopy of the ocular surface. The ocular surface. 2006;4(2):81-93.

[22] Knappe S, Stave J, Guthoff RF. [Epidemic keratoconjunctivitis. In vivo images of corneal structures with the confocal Rostocker laser scanning microscope (RLSM)]. Der Ophthalmologe : Zeitschrift der Deutschen Ophthalmologischen Gesellschaft. 2005;102(8):798-801.

[23] Scheimpflug T. Der photoperspektrograph und seine anwendung. Photogr Korr. 1906;43:516–31.

[24] Drews RC. Depth of Field in Slit Lamp Photography. An Optical Solution Using the Scheimpflug Principle. Ophthalmologica Journal international d'ophtalmologie International journal of ophthalmology Zeitschrift fur Augenheilkunde. 1964;148:143-50.

[25] Niesel P. [Slit-lamp photography of lens for measurement purposes]. Ophthalmologica Journal international d'ophtalmologie International journal of ophthalmology Zeitschrift fur Augenheilkunde. 1966;152(5):387-95.

[26] Brown N. Slit-image photography. Transactions of the ophthalmological societies of the United Kingdom. 1970;89:397-408.

[27] Brown N. Quantitative slit-image photography of the lens. Transactions of the ophthalmological societies of the United Kingdom. 1972;92:303-7.

[28] OCULUS, Optikgeräte, G.m.b.H. http://www.pentacam.com/sites/index.php (accessed in 29 august 2013).

[29] Ziemer, Ophthalmic, Systems, AG. http://galilei.ziemergroup.com/key-features-g4.html (accesed in 29 august 2013).

[30] Holladay JT. Corneal topography using the Holladay Diagnostic Summary. Journal of cataract and refractive surgery. 1997;23(2):209-21.

[31] Belin MW, Ambrosio R, Jr. Corneal ectasia risk score: statistical validity and clinical relevance. Journal of refractive surgery. 2010;26(4):238-40.

[32] Huang D, Swanson EA, Lin CP, Schuman JS, Stinson WG, Chang W, et al. Optical coherence tomography. Science. 1991;254(5035):1178-81.

[33] Izatt JA, Hee MR, Swanson EA, Lin CP, Huang D, Schuman JS, et al. Micrometer-scale resolution imaging of the anterior eye in vivo with optical coherence tomography. Archives of ophthalmology. 1994;112(12):1584-9.

[34] Maeda N. Optical coherence tomography for corneal diseases. Eye & contact lens. 2010;36(5):254-9.

[35] Yasuno Y, Madjarova VD, Makita S, Akiba M, Morosawa A, Chong C, et al. Three-dimensional and high-speed swept-source optical coherence tomography for in vivo investigation of human anterior eye segments. Optics express. 2005;13(26):10652-64.

[36] Dada T, Sihota R, Gadia R, Aggarwal A, Mandal S, Gupta V. Comparison of anterior segment optical coherence tomography and ultrasound biomicroscopy for assessment of the anterior segment. Journal of cataract and refractive surgery. 2007;33(5): 837-40.

[37] Jancevski M, Foster CS. Anterior segment optical coherence tomography. Seminars in ophthalmology. 2010;25(5-6):317-23.

[38] Goldsmith JA, Li Y, Chalita MR, Westphal V, Patil CA, Rollins AM, et al. Anterior chamber width measurement by high-speed optical coherence tomography. Ophthalmology. 2005;112(2):238-44.

[39] Doors M, Cals DW, Berendschot TT, de Brabander J, Hendrikse F, Webers CA, et al. Influence of anterior chamber morphometrics on endothelial cell changes after phakic intraocular lens implantation. Journal of cataract and refractive surgery. 2008;34(12):2110-8.

[40] Mohamed S, Lee GK, Rao SK, Wong AL, Cheng AC, Li EY, et al. Repeatability and reproducibility of pachymetric mapping with Visante anterior segment-optical coherence tomography. Investigative ophthalmology & visual science. 2007;48(12): 5499-504.

[41] Lai MM, Tang M, Andrade EM, Li Y, Khurana RN, Song JC, et al. Optical coherence tomography to assess intrastromal corneal ring segment depth in keratoconic eyes. Journal of cataract and refractive surgery. 2006;32(11):1860-5.

[42] Choi CY, Youm DJ, Kim MJ, Tchah H. Changes in central corneal thickness of preserved corneas over time measured using anterior segment optical coherence tomography. Cornea. 2009;28(5):536-40.

[43] Lim LS, Aung HT, Aung T, Tan DT. Corneal imaging with anterior segment optical coherence tomography for lamellar keratoplasty procedures. American journal of ophthalmology. 2008;145(1):81-90.

[44] Wylegala E, Nowinska A. Usefulness of anterior segment optical coherence tomography in Descemet membrane detachment. European journal of ophthalmology. 2009;19(5):723-8.

[45] Hong JP, Kim TI, Chung JL, Huang D, Cho HS, Kim EK. Analysis of deposit depth and morphology in granular corneal dystrophy type 2 using fourier domain optical coherence tomography. Cornea. 2011;30(7):729-38.

[46] Wylegala E, Dobrowolski D, Nowinska A, Tarnawska D. Anterior segment optical coherence tomography in eye injuries. Graefe's archive for clinical and experimental ophthalmology = Albrecht von Graefes Archiv fur klinische und experimentelle Ophthalmologie. 2009;247(4):451-5.

[47] Konstantopoulos A, Kuo J, Anderson D, Hossain P. Assessment of the use of anterior segment optical coherence tomography in microbial keratitis. American journal of ophthalmology. 2008;146(4):534-42.

[48] Pavlin CJ, Harasiewicz K, Sherar MD, Foster FS. Clinical use of ultrasound biomicroscopy. Ophthalmology. 1991;98(3):287-95.

[49] Pavlin CJ, Harasiewicz K, Foster FS. Ultrasound biomicroscopy of anterior segment structures in normal and glaucomatous eyes. American journal of ophthalmology. 1992;113(4):381-9.

[50] Pavlin CJ, Sherar MD, Foster FS. Subsurface ultrasound microscopic imaging of the intact eye. Ophthalmology. 1990;97(2):244-50.

[51] Dada T, Gadia R, Sharma A, Ichhpujani P, Bali SJ, Bhartiya S, et al. Ultrasound biomicroscopy in glaucoma. Survey of ophthalmology. 2011;56(5):433-50.

[52] Arun D, Hayden BC, Pavlin CJ. Ophthalmologic Ultrasound, An Issue of Ultrasound Clinics, 1e (The Clinics: Radiology): Saunders; 2008.

[53] Pavlin CJ, Foster FS. Ultrasound biomicroscopy in glaucoma. Acta ophthalmologica Supplement. 1992(204):7-9.

[54] Potash SD, Tello C, Liebmann J, Ritch R. Ultrasound biomicroscopy in pigment dispersion syndrome. Ophthalmology. 1994;101(2):332-9.

[55] Pavlin CJ, Easterbrook M, Harasiewicz K, Foster FS. An ultrasound biomicroscopic analysis of angle-closure glaucoma secondary to ciliochoroidal effusion in IgA nephropathy. American journal of ophthalmology. 1993;116(3):341-5.

[56] Yamamoto T, Sakuma T, Kitazawa Y. An ultrasound biomicroscopic study of filtering blebs after mitomycin C trabeculectomy. Ophthalmology. 1995;102(12):1770-6.

[57] Milner MS, Liebmann JM, Tello C, Speaker MG, Ritch R. High-resolution ultrasound biomicroscopy of the anterior segment in patients with dense corneal scars. Ophthalmic surgery. 1994;25(5):284-7.

[58] Pavlin CJ, Easterbrook M, Hurwitz JJ, Harasiewicz K, Eng P, Foster FS. Ultrasound biomicroscopy in the assessment of anterior scleral disease. American journal of ophthalmology. 1993;116(5):628-35.

[59] Gentile RC, Pavlin CJ, Liebmann JM, Easterbrook M, Tello C, Foster FS, et al. Diagnosis of traumatic cyclodialysis by ultrasound biomicroscopy. Ophthalmic surgery and lasers. 1996;27(2):97-105.

[60] Berinstein DM, Gentile RC, Sidoti PA, Stegman Z, Tello C, Liebmann JM, et al. Ultrasound biomicroscopy in anterior ocular trauma. Ophthalmic surgery and lasers. 1997;28(3):201-7.

[61] Deramo VA, Shah GK, Baumal CR, Fineman MS, Correa ZM, Benson WE, et al. Ultrasound biomicroscopy as a tool for detecting and localizing occult foreign bodies after ocular trauma. Ophthalmology. 1999;106(2):301-5.

[62] Pavlin CJ, McWhae JA, McGowan HD, Foster FS. Ultrasound biomicroscopy of anterior segment tumors. Ophthalmology. 1992;99(8):1220-8.

[63] THE, OPHTHALMIC, PHOTOGRAPHERS', SOCIETY, INC. Fundus Photography Overview. Available from: http://www.opsweb.org/?page=fundusphotography (accesed in 29.08.2013).

[64] Optos PLC D, Scotland KY11 8GR UK. Available from: http://www.optos.com/en/Products/Retinal-imaging-products/Ultra-widefield-imaging/ (accesed in 31.12.2013).

[65] Baeryer Av. Uber ein neue Klasse van farbstoffen. Der Deutschen Chem Ges. 1871(4): 555.

[66] Maclean AL, Maumenee AE. Hemangioma of the Choroid. Transactions of the American Ophthalmological Society. 1959;57:171-94.

[67] Anand R. Fluorescein angiography. Part 1: Technique and normal study. Journal of ophthalmic nursing & technology. 1989;8(2):48-52.

[68] Brancato R, Trabucchi G. Fluorescein and indocyanine green angiography in vascular chorioretinal diseases. Seminars in ophthalmology. 1998;13(4):189-98.

[69] Cavallerano AA. Ophthalmic fluorescein angiography. Optometry clinics : the official publication of the Prentice Society. 1996;5(1):1-23.

[70] Bloome MA. Fluorescein angiography: risks. Vision research. 1980;20(12):1083-97.

[71] Jennings BJ, Mathews DE. Adverse reactions during retinal fluorescein angiography. Journal of the American Optometric Association. 1994;65(7):465-71.

[72] Kelley JS. Fluorescein angiography: techniques and toxicity. International ophthalmology clinics. 1977;17(2):25-33.

[73] Yannuzzi LA, Rohrer KT, Tindel LJ, Sobel RS, Costanza MA, Shields W, et al. Fluorescein angiography complication survey. Ophthalmology. 1986;93(5):611-7.

[74] Halperin LS, Olk RJ, Soubrane G, Coscas G. Safety of fluorescein angiography during pregnancy. American journal of ophthalmology. 1990;109(5):563-6.

[75] J. Fernando Arevalo. Fluorescein Angiography: General Principles and Interpretation. Retinal Angiography and Optical Coherence Tomography: Springer; 2009.

[76] Ó. G. Björnsson RM, and V. S. Chadwick. Physicochemical studies of indocyanine green (ICG): absorbance/concentration relationship, pH tolerance and assay precision in various solvents. Experientia. 1982;38(12):1441–2.

[77] Engel E, Schraml R, Maisch T, Kobuch K, Konig B, Szeimies RM, et al. Light-induced decomposition of indocyanine green. Investigative ophthalmology & visual science. 2008;49(5):1777-83.

[78] Hayashi K, Hasegawa Y, Tokoro T. Indocyanine green angiography of central serous chorioretinopathy. International ophthalmology. 1986;9(1):37-41.

[79] Klais CM, Ober MD, Yannuzzi LA. Indocyanine Green Angiography: General Aspects and Interpretation. In: Arevalo JF, editor. Retinal Angiography and Optical Coherence Tomography: Springer; 2009.

[80] Benya R, Quintana J, Brundage B. Adverse reactions to indocyanine green: a case report and a review of the literature. Catheterization and cardiovascular diagnosis. 1989;17(4):231-3.

[81] Gilmore DM, Khullar OV, Jaklitsch MT, Chirieac LR, Frangioni JV, Colson YL. Identification of metastatic nodal disease in a phase 1 dose-escalation trial of intraoperative sentinel lymph node mapping in non-small cell lung cancer using near-infrared imaging. The Journal of thoracic and cardiovascular surgery. 2013;146(3):562-70.

[82] Wolf S, Arend O, Schulte K, Reim M. Severe anaphylactic reaction after indocyanine green fluorescence angiography. American journal of ophthalmology. 1992;114(5): 638-9.

[83] Orth DH, Patz A, Flower RW. Potential clinical applications of indocyanine green choroidal angiography--preliminary report. Eye, ear, nose & throat monthly. 1976;55(1):15-28, 58.

[84] Bischoff PM, Flower RW. Ten years experience with choroidal angiography using indocyanine green dye: a new routine examination or an epilogue? Documenta ophthalmologica Advances in ophthalmology. 1985;60(3):235-91.

[85] Heidelberg, Engineering, Inc. http://www.heidelbergengineering.com/us/products/hrt-glaucoma-module/hrt-product-specifications/ (accesed in 29.08.2013).

[86] Heidelberg, Engineering, Inc. http://www.heidelbergengineering.com/us/wp-content/uploads/2106_Product%20Lit_HRA%20wBluePeak_Product%20Sheet_v2.pdf (accesed in 29.08.2013).

[87] Optos. plc. http://www.optos.com/en-US/Products/Retinal-imaging-products/OCT-imaging/ (accesed in 31.12. 2013).

[88] Adhi M, Duker JS. Optical coherence tomography--current and future applications. Curr Opin Ophthalmol. 2013;24(3):213-21.

[89] Leitgeb R, Hitzenberger C, Fercher A. Performance of fourier domain vs. time domain optical coherence tomography. Optics express. 2003;11(8):889-94.

[90] Grulkowski I, Liu JJ, Potsaid B, Jayaraman V, Lu CD, Jiang J, et al. Retinal, anterior segment and full eye imaging using ultrahigh speed swept source OCT with vertical-cavity surface emitting lasers. Biomedical optics express. 2012;3(11):2733-51.

[91] Srinivasan VJ, Huber R, Gorczynska I, Fujimoto JG, Jiang JY, Reisen P, et al. High-speed, high-resolution optical coherence tomography retinal imaging with a frequency-swept laser at 850 nm. Optics letters. 2007;32(4):361-3.

[92] Huber R, Adler DC, Srinivasan VJ, Fujimoto JG. Fourier domain mode locking at 1050 nm for ultra-high-speed optical coherence tomography of the human retina at 236,000 axial scans per second. Optics letters. 2007;32(14):2049-51.

[93] Povazay B, Bizheva K, Hermann B, Unterhuber A, Sattmann H, Fercher A, et al. Enhanced visualization of choroidal vessels using ultrahigh resolution ophthalmic OCT at 1050 nm. Optics express. 2003;11(17):1980-6.

[94] Wang Y, Lu A, Gil-Flamer J, Tan O, Izatt JA, Huang D. Measurement of total blood flow in the normal human retina using Doppler Fourier-domain optical coherence tomography. The British journal of ophthalmology. 2009;93(5):634-7.

[95] Haouchine B, Massin P, Tadayoni R, Erginay A, Gaudric A. Diagnosis of macular pseudoholes and lamellar macular holes by optical coherence tomography. American journal of ophthalmology. 2004;138(5):732-9.

[96] Hillenkamp J, Kraus J, Framme C, Jackson TL, Roider J, Gabel VP, et al. Retreatment of full-thickness macular hole: predictive value of optical coherence tomography. The British journal of ophthalmology. 2007;91(11):1445-9.

[97] Barak Y, Ihnen MA, Schaal S. Spectral domain optical coherence tomography in the diagnosis and management of vitreoretinal interface pathologies. Journal of ophthalmology. 2012;2012:876472.

[98] Fung AE, Lalwani GA, Rosenfeld PJ, Dubovy SR, Michels S, Feuer WJ, et al. An optical coherence tomography-guided, variable dosing regimen with intravitreal ranibizumab (Lucentis) for neovascular age-related macular degeneration. American journal of ophthalmology. 2007;143(4):566-83.

[99] Goebel W, Kretzchmar-Gross T. Retinal thickness in diabetic retinopathy: a study using optical coherence tomography (OCT). Retina. 2002;22(6):759-67.

[100] Sanchez-Tocino H, Alvarez-Vidal A, Maldonado MJ, Moreno-Montanes J, Garcia-Layana A. Retinal thickness study with optical coherence tomography in patients with diabetes. Investigative ophthalmology & visual science. 2002;43(5):1588-94.

[101] Mundt GH, Jr., Hughes WF, Jr. Ultrasonics in ocular diagnosis. American journal of ophthalmology. 1956;41(3):488-98.

[102] Baum G, Greenwood I. The application of ultrasonics locating techniques to ophthalmology; theoretic considerations and acoustic properties of ocular media. I. Reflective properties. American journal of ophthalmology. 1958;46(5 Part 2):319-29.

[103] Şahin ÖG. Central corneal thickness, axial length, intraocular pressure and visual field indices in patients with ocular hypertension. Gulhane Medical Journal. 2010;52(4):266-9.

[104] Ossoinig KC. Ruling out posterior segment lesions with echography. International ophthalmology clinics. 1978;18(2):117-20.

[105] Lieb WE, Cohen SM, Merton DA, Shields JA, Mitchell DG, Goldberg BB. Color Doppler imaging of the eye and orbit. Technique and normal vascular anatomy. Archives of ophthalmology. 1991;109(4):527-31.

[106] Lieb WE, Shields JA, Cohen SM, Merton DA, Mitchell DG, Shields CL, et al. Color Doppler imaging in the management of intraocular tumors. Ophthalmology. 1990;97(12):1660-4.

[107] Baxter GM, Williamson TH. Color Doppler flow imaging in central retinal vein occlusion: a new diagnostic technique? Radiology. 1993;187(3):847-50.

[108] Romero JM, Finger PT, Rosen RB, Iezzi R. Three-dimensional ultrasound for the measurement of choroidal melanomas. Archives of ophthalmology. 2001;119(9): 1275-82.

[109] Naik MN, Tourani KL, Sekhar GC, Honavar SG. Interpretation of computed tomography imaging of the eye and orbit. A systematic approach. Indian journal of ophthalmology. 2002;50(4):339-53.